

Single-Molecule Techniques
in Biological and
Biophysical Research

Gerhard A. Blab

www.wiley.com/go/Blab

Single-Molecule Techniques in Biological and Biophysical Research

PROEFSCHRIFT

ter verkrijging van de graad van Doctor
aan de Universiteit Leiden,
op gezag van de Rector Magnificus Dr. D. D. Breimer,
hoogleraar in de faculteit der Wiskunde en
Natuurwetenschappen en die der Geneeskunde,
volgens besluit van het College voor Promoties
te verdedigen op donderdag 8 januari 2004
klokke 14.15 uur

door

Gerhard Adolf Blab

geboren te Wels, Oostenrijk, 7 November 1973

Promotiecommissie

Promotor: Prof. dr. Thomas Schmidt
Referent: Prof. dr. Horst Vogel (EPFL Lausanne)
Overige leden: dr. Thijs J. Aartsma
Prof. dr. Gregory S. Harms (Universität Würzburg)
Prof. dr. Niek van Hulst (Universiteit Twente)
Prof. dr. Peter H. Kes
Prof. dr. Michel Orrit

printed by Digital Printing Partners Utrecht BV

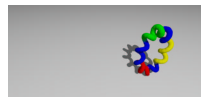
cover-art rendered with “Persistence of Vision Raytracer” (www.povray.org)

This thesis was typeset in L^AT_EX 2_ε.

Dedication

Dedicated to the memory of Professor Dr. Hansgeorg Schindler
(*September 27, 1943 – †August 28, 2001)

Möge er Antworten gefunden haben auf all seine “kurzen Fragen”.



DEDICATION

Professor Dr. Hansgeorg Schindler war der Gründer des Instituts für Biophysik an der Johannes Kepler Universität Linz, Österreich, und mein erster Lehrer auf diesem Gebiet.

Sein Markenzeichen, ein kurz vor dem Mittagessen geäußertes “Könnten Sie eben in mein Büro kommen, ich hätte eben eine kurze Frage!”, war der übliche Auftakt für lange Gespräche über den Fortgang der Arbeit im Labor. Er war sich auch der wirtschaftlichen Aspekte der Wissenschaft bewusst, und mit Hilfe des Landes Oberösterreich gründete er die “Upper Austrian Research”, einen Biotech-Betrieb zur Entwicklung und Vermarktung ultra-sensitiver Mikroskopiemethoden.

Am 28. August 2001 verstarb Professor Schindler an den Folgen eines Freizeitunfalls während eines Urlaubs in Frankreich.

Professor Dr. Hansgeorg Schindler was the founder of the Biophysics institute at the Johannes Kepler University in Linz, Austria, as well as my first teacher in this field.

His trademark comment “Could you come to my office for a moment, I’ve just got a short question!”, uttered shortly before lunch, usually meant a long scientific discussion about the progress in the lab. He was also well aware of the commercial side of science. With financial help from the state of Upper Austria he founded the biotech company “Upper Austrian Research”, whose aim is to develop and market ultra-sensitive microscopy methods.

Professor Schindler died on August 28, 2001, in an accident occurring during a vacation in France.

Contents

Dedication	iii
1 Introduction	1
1.1 Advancements in Microscopy	2
1.1.1 From <i>in vitro</i>	2
1.1.2 ...to <i>in vivo</i>	3
1.2 Theory	5
1.3 Single Fluorophore Markers	9
1.3.1 Shortfalls	9
1.3.2 Advantages	10
1.4 Producing Fluorescent Samples	11
1.4.1 Artificial Fluorophores	11
1.4.2 Genetic Modification	12
1.4.3 Autofluorescent Proteins	13
1.5 Scope of the Thesis	15
1.5.1 Two-Photon Excitation of Fluorescent Proteins . . .	15
1.5.2 Single-Molecule Studies of a Membrane Protein . . .	16

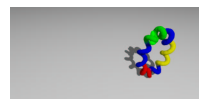
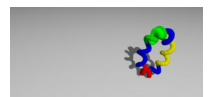


TABLE OF CONTENTS

1.5.3	High Sensitivity DNA Assay	18
1.5.4	Simultaneous Imaging and Spectroscopy	19
2	Two-Photon Fluorescence	31
2.1	Abstract	31
2.2	Introduction	32
2.3	Experimental Section	34
2.3.1	Sample Preparation	34
2.3.2	Two Photon Excitation	35
2.3.3	Measurement of Two-Photon Action Cross-Sections	35
2.4	Results and Discussion	36
2.5	Conclusions	40
2.6	Acknowledgement	41
3	Single Molecule Studies of β_2AR	51
3.1	Abstract	51
3.2	Introduction	52
3.3	Experimental Section	54
3.3.1	Single Molecule Microscopy	54
3.3.2	Cell Preparation	55
3.3.3	Stimulation Assays	55
3.3.4	Computer Simulations	56
3.3.5	Stoichiometric Analysis	56
3.4	Results and Discussion	57
3.5	Conclusions	61
3.6	Acknowledgment	62

4 High Sensitivity DNA Assay	73
4.1 Abstract	73
4.2 Introduction	74
4.3 Experimental section	75
4.3.1 RCR template and probes	75
4.3.2 High sensitivity detection	75
4.4 Results	77
4.5 Discussion	81
4.6 Acknowledgement	82
5 Imaging and Spectroscopy	93
5.1 Abstract	93
5.2 Introduction	94
5.3 Experimental Setup	95
5.4 Results and Discussion	96
5.4.1 Calibration	96
5.4.2 Nanometer-sized fluorescent beads	97
5.4.3 COBRA-FISH-stained mouse chromosomes	98
5.5 Conclusions	100
5.6 Acknowledgments	100
Summaries	107
Curriculum Vitae	117
Nawoord	119



Alle Kriegsherren haben
einen gemeinsamen Feind:
die Wahrheit.

All warlords have one com-
mon enemy: the Truth.

Kein Volk ist besser oder
schlechter als dein eigenes.

No people are better or
worse than your own.

Jeder Krieg ist eine Nieder-
lage. Denn Krieg ver-
nichtet Leben.

The outcome of every war
is a defeat, because war de-
stroys life.

Wer Kriege im Namen
Gottes führt, ist stets des
Teufels.

Anyone who wages war in
the name of God will al-
ways end up in hell.

Es gibt weder gerechte
noch heilige Kriege.

There are no such things as
Just or Holy Wars.

Kurt Tucholsky (1890 – 1935)
“Wenn sie wieder lügen”

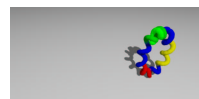
Chapter 1

Introduction

Long before Richard P. Feynman brought the world of nanostructures into the scientific spotlight by coining the phrase “There’s plenty of room at the bottom,” researchers have tried to elucidate with varying degrees of success what this “bottom” actually looks like.

Since the early days of microscopy, when microscopes consisted of relatively simple lens systems, the aim was to find more detail, reach higher resolution, as every new insight gained by resolving smaller detail will immediately lead to new questions. When Anton van Leeuwenhoek discovered the first protozoa in 1674 or Schleiden and Schwann proposed cells as building blocks of animals (1838), the question arose what these protozoa and cells made were of.

In the search for images with greater and greater detail, scientist were continually forced to overcome barriers set by their equipment. When the technical circumstances were right and optical systems could be manufactured reproducibly with great accuracy, the barrier shifted toward limits



set by the wave nature of light. These resolution limits are determined by the wavelength, λ , of light, giving access to length scales on the order of $\lambda/2$.

A more accurate value for the resolution is $1.22\frac{\lambda}{2NA}$, derived from the Fraunhofer diffraction of a circular aperture for a given wavelength λ and a numerical aperture of the objective NA. The theoretical discussion of the resolving power of a microscope by Abbé [1] dates back to the late 19th century. A detailed overview of microscopy methods and basics can be found in Pawlay [2] or Abramowitz [3]. A historical overview is given in Alberts et al. [4].

1.1 Advancements in Microscopy

1.1.1 From *in vitro*...

	wide-field	confocal
lateral	$0.52 \frac{\lambda}{NA}$	$0.37 \frac{\lambda}{NA}$
axial	$1.77 \frac{\lambda}{NA^2}$	$1.28 \frac{\lambda}{NA^2}$

Table 1.1: The Full-Width-Half-Maximum (FWHM) of the point-spread functions of optical wide-field microscopy and confocal microscopy.

Technical advances have allowed to shift this barrier set by the wavelength of light further to smaller and smaller structures, by using shorter and shorter wavelengths in the ultra-violet part of the spectrum, or by applying new focusing techniques such as confocal[2], and 4Pi-confocal[5]. Alternatively one can also employ multi-photon processes[6, 7], Point-Spread Function (PSF)-

engineering[8] or computational methods to evaluate finer details of a specimen. A way to truly break the wavelength-limit is the use of near-field

methods[9].

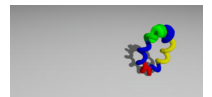
Consequently one can leave the domain of classical optics altogether and use an electron microscope, gaining the power to resolve single atoms in a lattice.

The price for these advantages, however, was to abandon biologically benign sample conditions and use harmful radiation (UV) or measure in vacuum (EM). These treatments of biological material disturb biological processes heavily, rendering most measurements to actually being done *in mortui*.

1.1.2 ...to *in vivo*

New methods had to be developed to overcome the need for destructive preparations and return to more biologically relevant conditions. A viable means to do this was to literally feel instead of look. Atomic Force Microscopy (AFM) uses a sharpened needle with a tip radius of only a few nanometers and a highly advanced force feedback to “feel” with resolutions down to sub-nanometers. Even under non-ideal circumstances this method gives access to proteins and even subunits thereof.

However, this method has its drawbacks as it is restricted to the surface of a given sample. On the other hand, the tactile approach allows to gain more than just topographical information. It will also reveal details about specific and unspecific interactions between the sample surface and the clean or coated tip, and measure the elastic properties of the sample. In the case of STM[10], which works on similar methods, yet with a current feedback to ascertain the topography, it is even possible to probe the electrical properties of e.g. ion channels or ion pumps in biological



membranes[11].

Single molecule fluorescence microscopy¹ is an alternative way to gain positional information below the resolution barrier set by the wavelength of light. The first report of the detection of a single biological molecule, an antibody tagged with about 100 fluorophores[15, 16] dates to 1976. Since then the sensitivity of the detection apparatus has been refined so that today the detection of the fluorescence emitted by a single fluorophore can be localized and quantified[17]

As a single fluorophore is essentially a point source on the length scale of resolution for a light microscopy, one can accurately pinpoint the center of the radial point-spread function, $h(u, v)$

$$h(u, v) = I(v) \equiv (\pi N) \left(\frac{2J_1(v)}{v} \right)^p \quad (1.1)$$

where $v = \frac{2\pi}{\lambda} r \cdot \text{NA}$ is the optical coordinate in radial, and $u = \frac{2\pi}{\lambda} z \frac{\text{NA}^2}{n}$ axial direction, $N = \frac{a^2}{\lambda f}$ the Fresnel number, λ the wavelength of light used, and a , f , NA are the aperture size, focal length and numerical aperture of the objective. $J_1(v)$ is the Bessel function of the first kind. The power p in equation 1.1 is determined by the type of microscopy used, i.e. 2 for conventional and 4 for confocal, in effect giving the latter a 30% better resolution.

As mentioned before, in the case of a single emitting fluorophore - or several fluorophores confined to a space much smaller than the resolution mentioned above - one can localize the position of this fluorescent marker with an accuracy much higher than the actual resolution of the microscope[18].

¹for a general overview over the field of single molecule fluorescence microscopy, please refer to the reviews by Moerner and Orrit [12], Weiss [13], and Sako and Yanagida [14].

A closed form for the estimation of the localization accuracy is presented by Thompson et al. [19], taking into account the spatial sampling of the detector (pixel size, a), the background noise b , the standard deviation of the point-spread function s and the number of collected photons N :

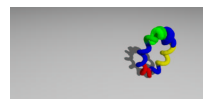
$$\langle (\Delta x)^2 \rangle = \frac{s^2 + \frac{a^2}{12}}{N} + \frac{8\pi s^4 b^2}{a^2 N^2}. \quad (1.2)$$

For the typical background in *in vivo* systems and the technical parameters of our imaging system, we can reach an accuracy of about 40 nm. Recent studies by Yildiz et al. [20] even show that *in vitro* an accuracy of down to 1.5 nm can be achieved.

In recent years the focus of imaging biophysics has shifted from “how” to “what”. The techniques have grown ever more sophisticated and robust, the ultimate sensitivity of single molecules has been obtained, the know-”how” is there. Now these methods have to be applied to biological research.

1.2 Theory of Single Molecule Fluorescence

A fluorophore can generally be described in terms of a four-level system as schematically shown in 1.1. The intensity dependent excitation rate $k_{exc} = \sigma(\lambda)I$ raises electrons from the ground state $|G\rangle$ to a vibrational level in the excited state $|E\rangle$. A fast relaxation ($\lesssim 1$ ps) leaves the electron in the lowest excited singlet level, from which it can return to the ground state with a rate of $k_s = 1/\tau_s$ or switch over to a triplet state $|T\rangle$ in a process designated “Inter System Crossing” (ISC). This process is spin forbidden, as both ground and excited state have spin $S = 0$, while the triplet has



$S = 1$, but can occur by mediation of spin-orbit coupling.²

As the return from the triplet to the ground state is obviously also spin-forbidden, it is usually several orders of magnitude slower than the decay from the excited state. If a photon is emitted from the triplet state, the process is called phosphorescence. In principle, both fluorescence and phosphorescence can occur in the same molecule, but due to the slow rate of phosphorescence, non-radiative relaxation from the triplet to the ground state is often the dominant process.

Gaseous benzene, for example will fluoresce upon excitation in the UV ($\lambda_{ex} > 260$ nm) at a wavelength around 300 nm. If benzene is frozen in a glassy matrix, phosphorescence is observable around 340 nm.

Furthermore, the molecule can undergo an irreversible change, causing it to cease fluorescing (k_b , “bleaching” or “photo-destruction”). Concerning the exact nature of this photo-destruction, literature is not completely clear. Some attribute this to a process originating from the excited singlet state[22], but most sources consider bleaching to be a process involving the triplet state[23], coupling to the triplet state of oxygen, which will form a highly reactive singlet oxygen which may destroy the chromophore. This latter model is the one implied in figure 1.1.

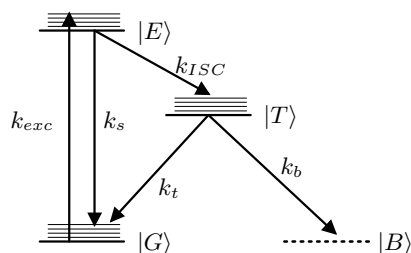


Figure 1.1: A simplified Jablonski diagram of the main energetic levels in a fluorophore. Typical values for the rate constants can be found in table 1.2.

²For a more complete overview on these processes as well as other de-excitation pro-

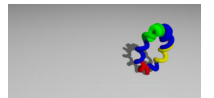
	eYFP	TMR
$\sigma \cdot 10^{-16} \text{ cm}^2$	2.5	1.9
$k_s \cdot 10^9 \text{ s}^{-1}$	0.27	0.48
$k_{ISC} \cdot 10^6 \text{ s}^{-1}$	*	14.2
$k_t \cdot 10^6 \text{ s}^{-1}$	*	0.5
$k_b \cdot 10^3 \text{ s}^{-1}$	0.29	0.14

Table 1.2: Rate constants for some fluorophores. the values for eYFP are taken from [23], those for Tetramethyl Rhodamine from [17]. (*) For eYFP the ratio $f_t = k_T/k_{ISC} = 0.08$ is known.

$$\frac{\partial N}{\partial t} = \begin{pmatrix} -k_{exc} & k_S & k_T & 0 \\ k_{exc} & -k_S - k_{ISC} & 0 & 0 \\ 0 & k_{ISC} & -k_T - k_B & 0 \\ 0 & 0 & k_B & 0 \end{pmatrix} \cdot N, N = \begin{pmatrix} N_G \\ N_E \\ N_T \\ N_B \end{pmatrix} \quad (1.3)$$

The kinetics of such a four-level system can be described by the differential equations given in 1.3. They can be solved numerically with small effort. Typical values for the rate constants are given in table 1.2. As the normalization condition $\sum_{j=G,E,T,B} N_j(t) = 1$ applies, the system is of rank three. The general solution will be a superposition of exponential functions $N_j = \sum_{i=1..3} C_{j,i} \cdot \exp(-\lambda_i t)$, where λ_i are the three eigenvalues of the matrix A and $C_{j,i}$ are constants determined by the normalized eigenvectors and initial conditions. While literature mentions closed solutions to this

cesses, please refer to Valeur [21].



system[see e.g. 22, 24, 25], it is usually assumed that bleaching is small or negligible, resulting in an easily solved second order system. The complete third order system of equation 1.3, however, can be solved analytically only by applying Cardano’s formula, which yields rather complex results which can not be simplified, making it very difficult to interpret them.

In the case of a small bleaching rate the fluorophore can be treated almost as a three-level system insofar that the population ratios of ground, excited and triplet state are close to the steady states of the simpler three-level system.

For the autofluorescent proteins, however, this simple model has severe limits, caused by the complicated photophysics of e.g. GFP and its variants[26]. In addition to the states mentioned before, the autofluorescent proteins undergo changes associated with protonation of the chromophore, causing them to either shift in wavelength or go into one of a number of extended “dark states”, remaining “silent” or unexcitable for times of a few microseconds to some hundreds of milliseconds. This also leads to the interesting observation that the mean bleaching time seems to be up to two orders of magnitude larger in bulk than for single-molecules[23], as the single molecule microscopy tends to lose track of molecules that stay dark for more than one image, typically less than 100 ms. Fluorescence Correlation Microscopy (FCS)[27, 28] has been used to show that this “blinking behavior” of autofluorescent proteins is present on different timescales.

1.3 Advantages and Shortfalls of Single Fluorophore Markers

1.3.1 Shortfalls

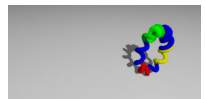
One of the most important limitation imposed on measurements with single fluorophores as markers is photo-bleaching, limiting the number of photons which will be emitted during the lifetime of a fluorophore.

$$F_{sm} = \frac{k^\infty \tau}{1 + \frac{I_S}{I_{ill}}} \cdot \left(1 - e^{-t_{ill}/\tau}\right) \quad (1.4)$$

Equation 1.4 gives the number of photons emitted, F_{sm} , as a function of the illumination time t_{ill} , the bleaching time τ , the maximal emission rate k^∞ , and the intensities of illumination (I_{ill}) and saturation (I_S). The bleaching factor ($1 - \exp(-t_{ill}/\tau)$) can be approximated to t_{ill} if the experimental conditions are chosen such that $t_{ill} \ll \tau$. This leads to the well known linear relation between collected signal F_{sm} and the illumination time.

In the case of autofluorescent proteins, and for the limit of individual fluorophores, the mean time before photobleaching is almost equal to the typical time of illumination[23]. The effect of bleaching during illumination can therefore not be neglected.

As mentioned before, Harms et al. [23] also showed that the bleaching time of fluorescent proteins appears to be higher when measured in bulk ($\tau_{bulk} = 112 \pm 3$ ms) than when measured on the level of single molecules ($\tau_{sm} = 3.5 \pm 0.5$ ms). A viable explanation for this seemingly inconsistency is the phenomenon of “blinking”, a process in which the fluorophore



converts into a long-lived “dark state” when excited. For all practical applications, we are not able to distinguish between a photo-damaged (bleached) molecule and a long-term inactive (“blinking”) fluorophore.

1.3.2 Advantages

The use of single-molecule markers allows biological processes to be studied at early stages, when only a small number of molecules is involved. Many signaling cascades will eventually produce a reaction which can be observed with simpler optical methods (i.e. a morphological change of the cell) or by chemical means (i.e. secretion of a substance).

Most processes, however, have a discrete starting point, like the recognition of a hormone by a membrane-bound receptor or the opening of a membrane channel in reaction to an applied voltage. It is of great interest to study these processes in these early moments, as chapter 3 explains for a G-protein-coupled receptor.

Furthermore, the study of molecules one at a time makes a synchronization unnecessary. Interactions will be observed as they happen, regardless of when they happen. This also allows easy access to possible subpopulations, which can be detected even if they are small. Unlike bulk experiments, the signal from a small population is not overwhelmed by the majority population in the single-molecule approach.

Finally, many cellular proteins occur in small and tightly regulated numbers. Every deviation, both above and below the normal level, can cause severe repercussions for the biological system. Studying individual, labeled proteins allows us to maintain this biologically relevant expression level and avoids the massive over-expression needed for many biochemical assays.

1.4 Producing Fluorescent Samples

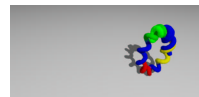
As the molecules of interest generally do not exhibit usable amount of fluorescence themselves, one has to label them before measurement[29]. There are many different ways to attach fluorescent labels. In the following I will introduce several of the possibilities.

1.4.1 Artificial Fluorophores

Artificial fluorophores come in a large variety of colors and with various protocols that allow the controlled attachment of the fluorophores to biomolecules.

Figure 1.5 show two examples of such fluorophores, tetramethyl rhodamine (TMR) and 4,4-difluoro-4-bora-3a,4a-diaza-*s*-indacene (BODIPY), which stand as generic models. By small modifications of the sidegroups, these fluorophores, as well as other, commercial fluorophores like Alexa-dyes or Cy-dyes, can be adapted for different wavelength regimes over the whole visible spectrum. The attachment process can be either covalent, as shown in figure 1.5C&D, where the widely used labeling of free sulfur and primary amines are shown. It has to be mentioned that these reactions again display a multitude of variations (addition of hydrocarbon spacers, modifications of the side chains) which will influence the specificity of the labeling, preferentially targeting certain sites in biomolecules.

Besides the direct labeling of biomolecules, one can also utilize non-covalent binding with antibodies, immunoglobulins (Ig), the specific interactions of avidin and biotin (biotinylated fluorophores) or nitrilotriacetic acid (NTA), which will chelate with a motif formed by six histidine amino



acids (his₆-tag) in the presence of nickel.

The advantages of labeling with artificial fluorophores – availability of protocols for many different biomolecules, high signal and stability of the fluorophore – far outweigh their disadvantages for most applications. Yet especially in the limit of single-molecule fluorescence, there are significant problems with these labeling schemes: Most biomolecules present more than one possible attachment site, rendering the labeling a statistical process. The labeling of the protein can also lead to loss of function. Furthermore most protocols require an excess of the label to ensure a satisfying labeling yield; this excess has to be removed before measurement if individual labeled entities are to be identified. It is also necessary to test that the presence of an excess of unbound, free fluorophores does not lead to unspecific binding.

1.4.2 Genetic Modification

As most proteins contain more than one possible labeling site, a method to increase the specificity of labeling is to use mutants of the proteins in which all but one labeling site are removed, or exactly one specific site is added. Obviously, such mutations have to be tested for their biological function. If several mutants are produced, which differ only in the position of the attached fluorophore, complex biological mechanisms, such as the function of motor proteins, can be studied[20] in great detail.

To obtain the protein, one can directly utilize the machinery inside a living cell. In a process called “transfection” a circular piece of DNA (plasmid) is introduced into the cell by means of a transfection agent. The plasmid contains the code of the mutant protein one wishes to study, a

promoter sequence which causes the cell to transcribe the DNA, and a gene encoding resistance to certain antibiotics, so that one can selectively kill all cells which do not contain the plasmid. After a few hours, the cell will start to produce the protein. Most proteins are purified from bacteria or yeast cells, as those are easier to grow in culture than mammalian cells.

This can also be taken one step further by not only changing a few amino acids but creating a “fusion protein”, a chimera of a small protein marker and a larger target protein. Again it is fundamental to ensure the functionality of this fusion protein. This method has become very important in recent years following the discovery of proteins which intrinsically exhibit fluorescence at a high level.

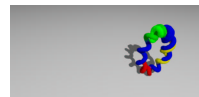
1.4.3 Autofluorescent Proteins

Already in 1962, Shimomura et al. [30] described the fluorescent properties of proteins found in the hydromedusa *Aequorea victoria* (figure 1.6). This finding was merely a footnote in their work to study the better known protein aequorin, a chemoluminescent protein, found in this jellyfish. The emission spectrum of the wild-type GFP peaked at 508 nm.

The break-through for the autofluorescent proteins³ came in with the cloning of the gene by Prasher et al. [32] in 1992 and the demonstration that GFP could be expressed in other organisms and still be fluorescent[33, 34].

Structurally, all fluorescent proteins derived from GFP share a motif of eleven β -sheets (forming the “ β -barrel”) with α -helices and coiled regions capping the structure (see figure 1.2). Another α -helix lies inside this barrel. In the wild-type GFP, three amino acids in the center of this helix, ⁶⁵Ser-⁶⁶Tyr-⁶⁷Gly, form the chromophore *p*-hydroxybenzylideneimidazolin-

³For a comprehensive review on the Green Fluorescent Protein, see also the review by Tsien [31].



one[33] after the protein obtains its tertiary structure[31]. This process is also referred to as “maturation” of the Fluorescent Protein and occurs within hours if oxygen is present. One consequence of the oxidative formation of the chromophore is the release of hydrogen peroxide, which could explain that high-level expression of GFP can affect the viability of cells.

To overcome limitations of the wild type protein, especially its tendency to dimerize, to yield low fluorescence, and to exhibit a strong dependence on the pH of the surrounding medium, “enhanced” or eGFPs were engineered by mutagenesis of the original wild type gene. Substitutions of the chromophoric amino acids as well as surrounding groups led to a variety of mutations with different absorption and emission properties. Today four groups of fluorescent proteins derived from the original *Aequorea*-GFP are available:

blue (eBFP; excitation: 360 nm, emission: 442 nm), cyan (eCFP; excitation: 452 nm, emission: 505 nm), green (eGFP; excitation: 488 nm, emission: 508 nm), and yellow (eYFP; excitation: 514 nm, emission: 527 nm). The actual number of distinct mutations is probably already close to a hundred.[data taken from: 31]

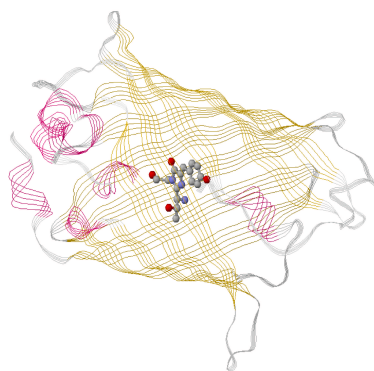


Figure 1.2: Molecular Model of GFP; the 11 β -sheets forming the barrel structure are shown as bands. The chromophore is located inside this barrel.

Source: Protein Data Bank, 1EMB

A recent addition is the even more red-shifted DsRed, a GFP-like protein derived from the tropical coral *Discosoma sp* (figure 1.7), which absorbs around 560 nm. While the application of this red variety has been limited due to its inherent formation of tetramers, enhanced, monomeric versions (mDsRed) have been described.[35]

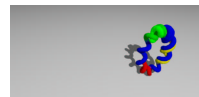
1.5 Scope of the Thesis

1.5.1 Application of Fluorescent Proteins with Two-Photon Excitation

In Chapter 2, the properties of the autofluorescent proteins are examined with two-photon excitation and compared to that of flavin. Flavin, while a weak fluorophore, is part of the cellular energy cycle and therefore highly abundant in living cells. In this study, flavin is used as a model for the cellular autofluorescence.[36]

Two-photon excitation is a non-linear process, in which a fluorophore absorbs two photons in rapid succession, each of which carries half the energy needed for the transition between ground state and excited state. The (informal) unit for the two-photon absorption cross-section is named after Maria Göppert-Mayer (1 GM = 10^{-50} cm⁴ s/photon), who predicted this process in 1931.[37]

Compared to the one-photon absorption cross-section ($\sigma = 10^{-16}$ cm²) the two-photon absorption cross-section is very small. Even as the probability for a two-photon event is dependent on the square of the laser intensity, one still needs an about six orders of magnitude higher intensity to obtain the same probability of absorption. Important is the num-



ber of photons of wavelength λ per Joule, which can be calculated by $N_{p\lambda} = \frac{\lambda}{hc} = \lambda \cdot 5.03 \cdot 10^{15}$ (λ in nm). A typical excitation intensity for one-photon fluorescence measurements is 1 kW/cm^2 , which corresponds to $N_{p, 514\text{nm}} \simeq 2.6 \cdot 10^{18}$ photons/ms/cm².

These comparatively large laser intensities can be achieved by a pulsed laser system which will generate short (100 fs) pulses with a very high peak power.

The basic advantage of two-photon excitation is based on the earlier observation that the two-photon absorption cross-section of a variety of fluorescent molecules scales super-linearly with the one-photon absorption cross-section[38]. Furthermore, due to the low absorption of infra-red radiation in biological materials, it is possible to image deep into tissue with negligible damage.

It was the hope to use autofluorescent proteins as single-molecule markers in *in vivo* two-photon-microscopy, which would have allowed to greatly reduce the background usually plaguing measurements. All autofluorescent proteins exhibited large two-photon action cross-sections σ_{TPE} , ranging from 8 GM (eCFP) to 40 GM (eGFP, see table 2.1 for full details), and unlike in the one-photon case all fluorescent proteins were clearly distinguishable from the much smaller signal of flavin ($\sigma_{TPE} = 0.4 \text{ GM}$). In conclusion, however, the rapid photo bleaching proved prohibitive[39] and does not allow their use as single-molecule markers under two photon excitation.

1.5.2 Single-Molecule Studies of a Membrane Protein

In chapter 3, stimulation of β_2 -adrenergic receptors (β_2 ARs) is studied

on the single-receptor level. The β_2 AR is a member of the family of G-protein-coupled receptors (GPCR, figure 1.3), which share a hepta-helical structure, are the largest class of cell-surface receptors, and are a major target for drug development.[for an overview see: 41] The β_2 AR is a receptor found in many different tissues and it mediates the action of catecholamines – neurotransmitters which are derived from tyrosine, such as dopamine and epinephrine – that produce relaxation of smooth muscles and vasodilatation.

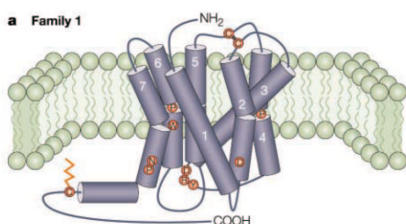


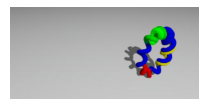
Figure 1.3: A model of a G-protein coupled receptor (GPCR). Common to all members of this large family are the seven transmembrane helices. Figure adapted from [40].

Universiteit Amsterdam. This construct was tested and found to have fully retained its biological function.

We set out to test the hypothesis that monomeric receptors are recruited into functional dimers upon stimulation. As the stoichiometry of individual entities on the cell membrane changes, their intensity will change

Especially the role of oligomerization of the receptors is a topic of great interest[42], as the exact function and mechanism behind the formation of homo- and hetero-dimers between closely related GPCRs in live cells is still under debate.

To study the oligomerization of the receptor with our highly sensitive single-molecule methods, we produced a β_2 AR-eYFP fusion protein in collaboration with the Department of Medicinal Chemistry at the Vrije



accordingly.[17]

To quantify the resulting intensity distributions (figure 3.2) we had to characterize the signal distribution from known monomeric YFP-fusion proteins and develop models to account for the bleaching and blinking behavior of the fluorescent proteins.

Computer simulations show that this is no trivial task, as for higher order aggregates (> 3) the intensity distributions of the oligomers start to smear out as shown in figure 3.4. It deviates markedly from the ideal of a multi-peaked distribution that can be found in model systems and for fluorophores which are stable longer than the average time of illumination.

Our measurements show that the β_2 AR can be found in a mostly dimeric state before stimulation and that it will form larger aggregates within less than one minute after stimulation. These aggregates remain stable on a timescale of minutes.

1.5.3 Technical Application of Single-Molecule Microscopy in DNA Research

In chapter 4 an application for rapid and separation-free detection of single base-pair mismatches of DNA is presented.

The method utilizes the high sensitivity of our setup to detect a strand of multiply labeled DNA against the background of excess labeled probe.

In contrast to existing methods like PCR (Polymerase Chain Reaction), which can also be used to detect variations in only one DNA base, this new technique does not require temperature cycling or cleaning steps to remove unbound probes.

This is made possible by Rolling Circle Amplification[43, 44] of spe-

cially designed “padlock”-probes, which generates a long, repeated, single-stranded piece of DNA upon recognition of a certain DNA sequence. The recognition step in this reaction is sensitive enough to be blocked by a single basepair mismatch. Figure 1.8 gives a schematic presentation of this technique.

The recognition site of the padlock probe is located on the ends of the DNA strand. Only if the template strand is matched perfectly a ligase will be able to ligate the two ends of the padlock, brought together by the recognition of the target. A circular piece of DNA is formed in this process. Addition of Φ 29 DNA polymerase will generate the long, repeated sequence of single-stranded DNA mentioned above.

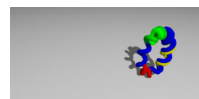
With repeat-length of up to 1000 copies, binding of fluorescently labeled oligo-nucleotides resulted in an extremely high localized signal, which was detected against a 1000-fold excess of free fluorescent probes.

In addition to the adaptation of the optical setup to allow the observation of a larger area ($100 \times 100 \mu\text{m}^2$), a flow system had to be implemented to screen larger amounts of sample in a fast, controlled and thereby reliable way.

1.5.4 Simultaneous Imaging and Spectroscopy

As the previous chapters concerned mainly the quantification and localization of single molecules, chapter 5 covers work on simultaneous localization and spectroscopic analysis of small, dilute fluorescent particles using a reflective blazed grating.

The technique described in this chapter was used in two distinct ways. It presents an enhancement of previously described methods[45], in which



two different fluorophores could be simultaneously observed using a wedge mirror. By using a blazed grating, I generalized this to an arbitrary number of fluorescent labels, only limited by the discrimination permitted from the resolution of the grating and the requirement of simultaneous excitation of the fluorophores.

One venue opened by this imaging spectroscopy method is the study of photosynthetic Light Harvesting Complexes at 4.2 K. Current practice is the identification of these LH-complexes by wide-field imaging, while the subsequent spectral analysis has to be done with confocal methods[46]. By using a grating, one can combine these steps, simultaneously obtaining the emission-spectra of a number of complexes.

In our experiments we characterize the sensitivity of the method by using 20 nm fluorescent latex beads with spectra in the yellow ($\lambda_{em} = 520$ nm) and red ($\lambda_{em} = 600$ nm), each giving a signal equivalent to ~ 180 fluorescein molecules. The emission spectra gained from such individual beads are in excellent agreement with bulk-spectra obtained of beads in solutions (figure 5.2).

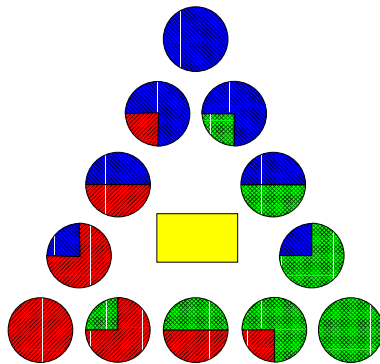
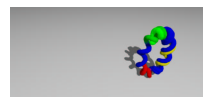


Figure 1.4: The COBRA-FISH labeling for $n = 3$, $r = 3$ and one binary label. The number of possible combination is 24, allowing each chromosome in the mouse genome to be labeled with a unique combination.

In a more application directed approach, we use this new technique to the karyotyping of mouse chromosomes. In a COBRA-FISH⁴ [47] stained sample each chromosome carries a defined combination of four fluorophores in specific ratios, thereby allowing to uniquely identify each chromosome.

Conventionally, the chromosomes are identified by consecutive imaging with different excitation and emission filter set to identify the component fluorochromes. With our new technique, a single exposure is enough, to read out the full information.

⁴**combined binary ratio - fluorescence in-situ hybridization.** A technique which allows to define a combinatory labeling by using n fluorochromes, only two of which are used simultaneously per target, in r different intermediate labeling ratios, i.e. for $r = 3$ this would be 0% (none), 25%, 50%, 75% and 100% (full) staining. m additional “binary” labels can be added, resulting in $n + \frac{r \cdot n!}{2^{(n-2)!}} \cdot 2^m$ distinct color codes (figure 1.4).



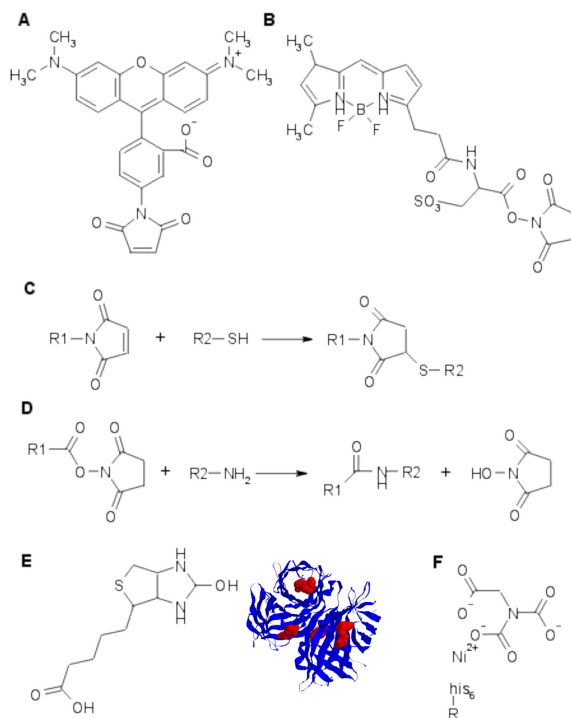
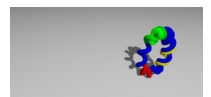


Figure 1.5: Two examples and reaction schematics of commercially available fluorophores for the labeling of biomolecules. Tetramethyl rhodamine-6-maleimide (**A**) will form a thioether with free sulphur groups (**C**), such as can be found in cysteine-residues of proteins. BODIPY-FL (**B**) contains a succinimidyl ester that will form a carboxamide (**D**) with primary amino groups. (**E**) shows a non-covalent binding based on the specific recognition of the small molecule biotin (left) by the tetrameric protein avidin (right). Yet another common method to attach or immobilize is the use of NTA, which will form a stable chelate with a his₆ motif of proteins in the presence of nickel (**F**). Source for the model of Avidin: Protein Data Bank, SWE1.



Copyright © Tim Hellier/imagequestmarine.com

Figure 1.6: The hydromedusa *Aequorea victoria* naturally contains the original Green Fluorescent Protein.



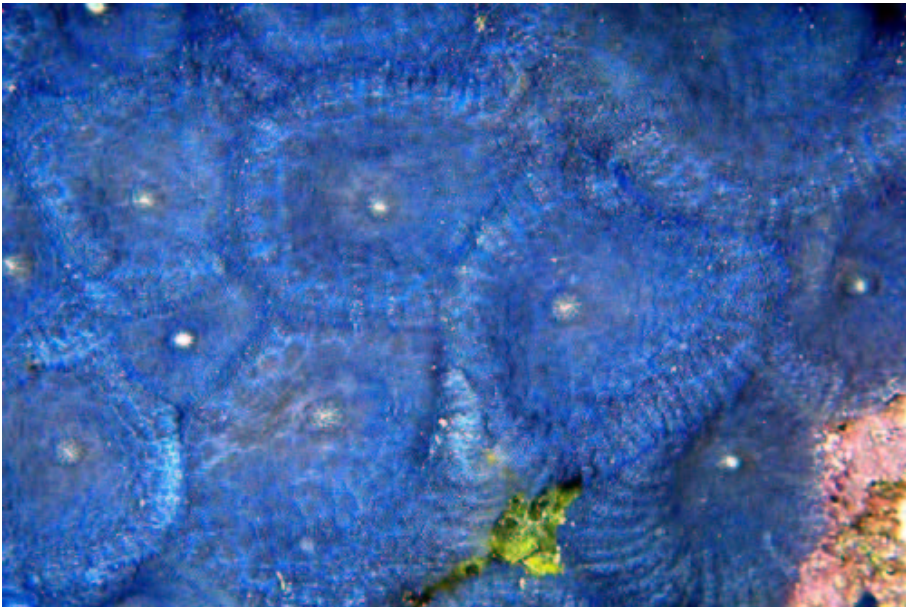


Figure 1.7: The coral *Discosoma sp* possesses a protein “DsRed” which is very similar in structure to the green fluorescent protein from *Aequoria victoria*, yet exhibits red fluorescence.

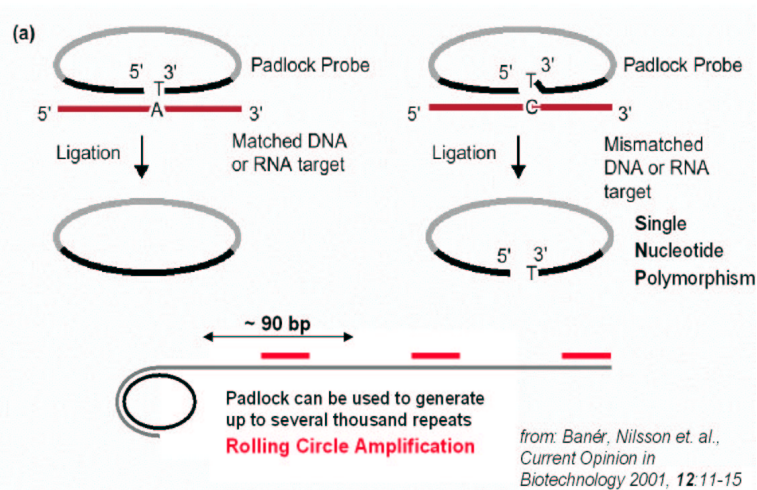
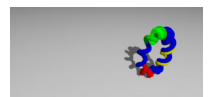


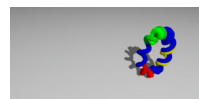
Figure 1.8: The Rolling Circle Replication (RCR) depends on the recognition of the target DNA by a padlock probe. The recognition sequence is located at either end of the padlock, so that in the case of a match the probe can be circularized by a DNA ligase. A single DNA-mismatch will prohibit this ligation. Φ 29 DNA polymerase was used to form a long, single-stranded DNA consisting of repeats of the 93 base pair padlock probe.



Bibliography

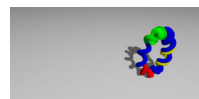
- [1] E Abbé. Beiträge zur Theorie des Mikroskops und der mikroskopischen Wahrnehmung. *Schultzes Arc. f. Mikr. Anat.*, 9:413–469.
- [2] JB Pawlay, editor. *Handbook of Biological Confocal Microscopy*. Plenum Press, 2nd edition, 1995.
- [3] M Abramowitz. Microscopy ressource center - primer. Internet Presentation, <http://www.olympusmicro.com/primer/>, 1997.
- [4] B Alberts, D Bray, Lewis J, Raff M, Roberts K, and Watson JD. *Molecular Biology of the Cell*, chapter 4. Garland Publishing, 3rd edition, 1994.
- [5] SW Hell and EHK Stelzer. Properties of a 4Pi-confocal fluorescence microscope. *J.Opt.Soc.Am. A*, 9:2159–2166, 1992.
- [6] W Denk, DW Piston, and WW Webb. *Handbook Of Biological Confocal Microscopy*, pages 445–457. Plenum Press, 1995.
- [7] C Xu, W Zipfel, JB Shear, RM Williams, and WW Webb. Multiphoton fluorescence excitation: new spectral windows for biological nonlinear microscopy. *PNAS (USA)*, 93(20):10763–10768, 1996.
- [8] TA Klar, S Jakobs, M Dyba, A Egner, and SW Hell. Fluorescence microscopy with diffraction resolution barrier broken by stimulated emission. *Proc. Nat. Acad. Sci (USA)*, 97(15):8206–8210, 2000.
- [9] DW Pohl, W Denk, and M Lanz. Optical stethoscope: Image recording with resolution $\lambda/20$. *Applied Physics Letters*, 44(7):651–653, 1984.
- [10] G Binning, H Rohrer, Ch Gerber, and E Weibel. Tunneling through a controllable vacuum gap. *Applied Physics Letters*, 40(2):178–180, 1982.
- [11] Stamouli A, JWM Frenken, TH Oosterkamp, RJ Cogdell, and TJ Aartsma. The electron conduction of photosynthetic protein complexes embedded in a membrane. *submitted*, 2004.
- [12] WE Moerner and M Orrit. Illuminating single molecules in condensed matter. *Science*, 283:1670–1676, 1999.

- [13] S Weiss. Fluorescence spectroscopy of single biomolecules. *Science*, 283:1676–1683, 1999.
- [14] Y Sako and T Yanagida. Single-molecule visualization in cell biology. *Nature Review Molecular Cell Biology*, 4(supplement):SS1–SS5, 2003.
- [15] T Hirschfeld. Optical microscopic observation of single small molecules. *Applied Optics*, 15(12):2965–2966, 1976.
- [16] T Hirschfeld. Quantum efficiency independence of the time integrated emission from a fluorescent molecule. *Applied Optics*, 15(12):3135–3138, 1976.
- [17] T Schmidt, GJ Schütz, W Baumgartner, HJ Gruber, and H Schindler. Characterization of photophysics and mobility of single molecules in a fluid lipid membrane. *Journal of Physical Chemistry*, 99:17662–17668, 1995.
- [18] N Bobroff. Position measurement with a resolution and noise-limited instrument. *Review of Scientific Instruments*, 57(6):1152–1157, 1986.
- [19] RE Thompson, DR Larson, and WW Webb. Precise nanometer localization analysis for individual fluorescent probes. *Biophysical Journal*, 82(5):2775–2783, May 2002.
- [20] A Yildiz, JN Forkey, SA McKinney, T Ha, YE Goldman, and PR Selvin. Myosin V walks hand-over-hand: Single fluorophore imaging with 1.5-nm localization. *Science*, 300(5628):2061–2065, 2003.
- [21] Bernard Valeur. *Molecular Fluorescence*. Wiley-VCH, 69469 Weinheim, Germany, 2002.
- [22] C Zander, J Enderlein, and Keller RA. *Single Molecule Detection in Solution, Methods and Applications*. Wiley-VCH, 1 edition, 2002.
- [23] GS Harms, L Cognet, PHM Lommerse, GA Blab, and T Schmidt. Autofluorescent proteins in single-molecule research: Applications to live cell imaging microscopy. *Biophysical Journal*, 80:2396–2408, 2001.
- [24] A Schönle and SW Hell. Far-field fluorescence microscopy with repetitive excitation. *Eur.Phys.J. D*, 6:283–290, 1999.
- [25] S Speiser, R van der Werf, and J Kommandeur. Photoquenching: The



- dependence of the primary quantum yield of a monophotonic laser-induced photochemical process on the intensity and duration of the exciting pulse. *Chemical Physics*, 1:297–305, 1973.
- [26] TMH Creemers, AJ Lock, V Subramaniam, TM Jovin, and S Völker. Three photoconvertible forms of green fluorescent protein identified by spectral hole-burning. *Nature Structural Biology*, 6:557–560, 1999.
- [27] EJG Peterman, S Brasselet, and WE Moerner. The fluorescence dynamics of single molecules of green fluorescent protein. *Journal of Physical Chemistry A*, 103:10553–10560, 1999.
- [28] P Schuille, S Kummer, AA Heikal, WE Moerner, and WW Webb. Fluorescence correlation spectroscopy reveals fast optical excitation-driven intramolecular dynamics of yellow fluorescent proteins. *PNAS (USA)*, 97(1):151–156, 2000.
- [29] A Miyawaki, A Sawano, and T Kogure. Lighting up cells: labeling proteins with fluorophores. *Nature Cell Biology*, 5(supplement):S1–S7, 2003.
- [30] O Shimomura, F Johnson, and Y Saiga. Extraction, purification and properties of aequorin, a bioluminescent protein from the luminous hydromedusa aequorea. *J. Cell. Comp. Physiol.*, 59:223–239, 1962.
- [31] RY Tsien. The green fluorescent protein. *Annu. Rev. Biochem.*, 67, 1998.
- [32] DC Prasher, VK Eckenrode, WW Ward, FG Prendergast, and MJ Cormier. Primary structure of the aequorea-victoria green-fluorescent protein. *Gene*, 111:229–233, 1992.
- [33] M Chalfie, Y Tu, G Euskirchen, WW Ward, and DC Prasher. Green fluorescent protein as a marker for gene-expression. *Science*, 263:8802–8805, 1994.
- [34] S Inouye and FI Tsujii. Evidence for redox forms of the aequorea green fluorescent protein. *FEBS Letters*, 341:277–280, 1994.
- [35] RE Campbell, Tour O, AE Palmer, PA Steinbach, GS Baird, DA Zacharias, and RY Tsien. A monomeric red fluorescent protein.

- PNAS (USA)*, 99(12):7877–7882, 2002.
- [36] RC Benson, RA Meyer, ME Zaruba, and GM McKhann. Cellular autofluorescence – is it due to flavins? *Journal of Histochemistry and Cytochemistry*, 27:44–48, 1979.
- [37] M Göppert-Mayer. Über Elementarakte mit zwei Quantensprüngen. *Annalen der Physik*, 9:273–295, 1931.
- [38] C Bubeck, A Grund, A Kaltbeizel, D Neder, A Mathy, and G Wegner. *Organic Molecules for Nonlinear Optics and Photonics*, pages 335–343. Kluwer Academic Publishing, 1991.
- [39] M Sonnleitner, GJ Schütz, and T Schmidt. Imaging individual molecules by two-photon excitation. *Chemical Physics Letters*, 300: 221–226, 1999.
- [40] SR George, BF O’Dowd, and SP Lee. G-protein-coupled receptor oligomerization and its potential for drug discovery. *Nature Reviews*, 1:808–820, October 2002.
- [41] KL Pierce, RT Premont, and RJ Lefkowitz. Seven-transmembrane receptors. *Nature Reviews of Molecular Cell Biology*, 3(9):639–650, 2002.
- [42] S Angers, A Salahpour, and M Bouvier. Dimerization: An emerging concept for g protein-coupled receptor ontogeny and function. *Annual Review of Pharmacology and Toxicology*, 42(1):409–435, 2002.
- [43] M Nilsson, H Malmgren, M Samiotaki, M Kwiatkowski, BP Chowdhary, and Landgren U. Padlock probes: Circularizing oligonucleotides for localized DNA detection. *Science*, 265:2085–2088, 1994.
- [44] M Nilsson, K Krejci, J Koch, M Kwiatkowski, P Gustavsson, and U Landgren. Padlock probes reveal single-nucleotide differences, parent of origin and in situ distribution of centromeric sequences in human chromosomes 13 and 21. *Nature Genetics*, 16:252–255, 1997.
- [45] L Cognet, GS Harms, GA Blab, PHM Lommerse, and T Schmidt. Simultaneous dual-color and dual-polarization imaging of single molecules. *Applied Physics Letters*, 77:4052, 2000.



- [46] A van Oijen, M Ketelaars, J Köhler, TJ Aartsma, and J Schmidt. Unraveling the electronic structure of individual photosynthetic pigment-protein complexes. *Science*, 285:400–402, 1999.
- [47] HJ Tanke, J Wiegand, RPM van Gijlswijk, V Bezrookove, H Pattenier, RJ Heetebrij, EG Talman, AK Raap, and J Vrolijk. New strategy for multi-colour fluorescence in situ hybridisation: COBRA: COmbined Binary RATio labeling. *European Journal of Human Genetics*, 7:2–11, 1999.

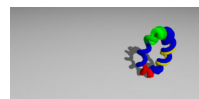
Chapter 2

Two-Photon Excitation Action Cross-Section of the Autofluorescent Proteins

The work described in this chapter has been published as “Two-Photon Excitation Action Cross Section of the Autofluorescent Proteins” in Chemical Physics Letters[1].

2.1 Abstract

We report on the values of the two-photon excitation action cross-sections of commercially available enhanced cyan, green, yellow and red fluorescent proteins. The two-photon absorption spectra are very similar in shape to those measured for one-photon absorption. However, they exhibit a significant blue shift, which is attributed to the participation of a vibrational



mode in the two-photon absorption process. The two-photon spectra are compared to that of flavine mononucleotide, which constitutes the main source of autofluorescence in mammalian cells. The definition of a relative detection yield between the autofluorescent proteins and flavine allows to quantify the applicability of autofluorescent proteins in two-photon single-molecule studies in living cells.

2.2 Introduction

Major innovations in recent years have largely revolutionised the fluorescence imaging of biological samples. Two photon excitation using near-infrared wavelength short laser-pulses increased the achievable penetration depth in thick samples, which for the first time renders imaging of thick tissues possible[2, 3]. In addition, the out-of-focus photodamage of the samples is essentially avoided which further facilitates reliable volume imaging of fluorescent samples.

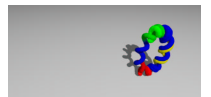
Another advancement came from the discovery of the autofluorescent proteins originating from the jellyfish *Aequorea victoria*[4]¹ and the coral *Discosoma sp*[6]. By fusing a specific protein with an autofluorescent protein, the functional imaging of complex processes in cells became possible for the first time: the role of microtubuli in mitosis[7], functional oligomerisation of cellular proteins[8], or changes in the intracellular Ca^{2+} -level[9, 10].

One advantage of the fluorescence labelling technique in comparison to bioconjugation is its extremely high sensitivity which makes experiments

¹For an overview of autofluorescent proteins see Tsien [5] and references therein.

feasible down to the level of a single molecule, opening a new avenue for cell biological and biophysical research. While the applicability of the autofluorescent proteins for single-molecule research *in vivo* has recently been demonstrated[8, 11, 12], its general application is still in early development. One major issue is the detectability of a single fluorophore within the autofluorescence background inside a living cell. The main component of this autofluorescent background are flavine molecules which are present at particularly high abundance of 100-1000 molecules per focal volume element[13]. Due to the broad absorption of flavine in the blue/green part of the visible spectrum the excitation spectra of the cellular autofluorescence strongly overlaps with the excitation spectra of the fluorescent proteins. For this reason, only the two most red-shifted varieties, the enhanced yellow fluorescent protein (eYFP) and the red fluorescent protein (DsRed), provide a significantly stronger wavelength discrimination compared to the flavines in wide-field single-molecule applications[11].

Here we report on the prospects of using two-photon excitation (TPE) in order to largely increase the signal-to-background ratio in our quest for general single-molecule detection of the autofluorescent proteins in live cells. The basic idea for two-photon excitation is resting on the earlier observation that the two-photon absorption cross-section of a variety of fluorescent molecules scales super-linearly with the one-photon absorption cross-section[14]. Hence, the ratio of the effective excitation rate of a fluorophore with high one-photon absorption cross-section, like the fluorescent proteins, and a fluorophore with a low one-photon absorption cross-section, like flavines, will be largely increased for two-photon excitation. Indeed our data show a super-linear scaling behaviour which has been previously de-



scribed only for small organic molecules. For exploitation and optimisation of the two-photon excitation scheme we have fully characterised and compared the two-photon spectroscopic properties of commercially available autofluorescent proteins and that of flavine mononucleotide. Our findings might lead to a novel strategy of two-photon imaging of single molecules using the autofluorescent proteins as markers.

2.3 Experimental Section

2.3.1 Sample Preparation

The autofluorescent proteins were purified as described previously[11]. In short, plasmids containing the coding sequences of the autofluorescent proteins with a C-terminal his₆-tag (peXFP, Clontech) were transformed into *E.coli* and cultured at 37°C. The cells were harvested, lysed and the fluorescent protein was extracted using a column of chelating sepharose (Pharmacia Biotech).

Concentrations of the fluorescent proteins were determined by measuring their absorption spectra. SDS-PAGE analysis revealed a correct molecular weight and an estimated purity of at least 95%.

25 μ l of stock solution of the fluorescent proteins and a stock solution of flavine mononucleotide were diluted in phosphate-buffered saline (PBS: 150mM NaCl, 15mM Na₂PO₄, pH7.4) to obtain a final concentration in the low μ M range. Fluoresceine was diluted from stock into distilled water (NaOH to adjust for pH > 11).

All fluorophore concentrations were controlled spectroscopically.

2.3.2 Two Photon Excitation

Femtosecond pulses from a Ti:sapphire laser (Tsunami, Spectra Physics) with a mean power of 1-200 mW (150 fs pulsewidth, 80 MHz repetition rate) were focussed by a 10 \times objective (Zeiss) into a quartz cuvette containing the solution. The focal spot had a diameter of approximately 100 μm .

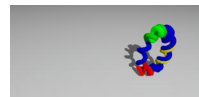
The fluorescence signal was discriminated from the excitation light by a 6 mm-thick blueglass filter (BG, Schott) and detected on an avalanche photodiode (SPCM-141, EG&G) under an angle of 90 $^\circ$. The overall detection efficiency of the entire setup was about 1%. Fluorescence signals were integrated over periods of 50 ms.

2.3.3 Measurement of Two-Photon Action Cross-Sections

In this study we report on the two-photon excitation (TPE) action cross-section σ_{TPE} , defined as the product of the two-photon absorption cross-section, $\chi^{(2)}$, and the fluorescence quantum yield, Φ .

All samples were measured at mean laser powers ranging from 1-200 mW (1-212 MW/cm 2 peak intensity) and up to 400 mW. The data were corrected for the background signal, $F_0 < 10$ kcps, which was obtained from the pure buffer solutions on excitation.

Since the measurement of absorption cross-sections in the two-photon case heavily depends on the spatial and temporal coherence of the excitation beam[15] a calibration against a reference spectrum was employed using the routine described in detail in Albota et al. [16]. In short, the fluorescence signal, F , was measured for the particular autofluorescent protein under study and compared to the fluorescence signal, F_{cal} , obtained from



fluoresceine for which the two-photon action cross-section, σ_{TPE}^{cal} , has been reported[16]:

$$\sigma_{TPE} = \frac{\eta^{cal}}{\eta} \cdot \frac{c^{cal}}{c} \cdot \frac{F - F_0}{F^{cal} - F_0} \cdot \sigma_{TPE}^{cal} \quad (2.1)$$

The collection efficiencies, η ($\eta=0.5\%$ for DsRed, $\eta=\eta_{cal}=1.1\%$ for all other fluorophores), and the respective sample concentrations, c , as obtained by one-photon absorption measurements on each sample were taken into consideration.

For wavelengths > 960 nm, where values for fluoresceine were lacking, the corrections were extrapolated from the 960 nm calibration value. The calibration procedure ensures that any effects such as the strong influence of spatial and temporal coherence of the excitation beam on the obtained results can be neglected.

2.4 Results and Discussion

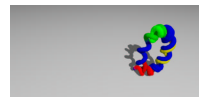
The foremost characteristic of two-photon induced fluorescence is the dependence of the signal on the square of the excitation intensity[17]. For each wavelength measured we have recorded a power series of the detected fluorescence signal for peak intensities between 1–424 MW/cm² (figure 2.1).

For all 84 experiments we found that the fluorescence signal, F , followed a power-law dependence on the excitation power, $F \propto I^\alpha$ with an average exponent of $\alpha = 1.92 \pm 0.17$ (mean \pm std). At the respective two-photon absorption maxima of the autofluorescent proteins, and thus at the highest signal-to-noise ratios, the average exponent was $\alpha = 2.00 \pm 0.03$ (figure 2.1). Hence, it can be safely concluded that the detected signals originated from a two-photon excitation process.

The TPE action cross-section spectra of the various autofluorescent proteins are given in figure 2.2 (data points) and are summarized in table 2.1. The maxima of the two-photon absorption spectra of the cyan (eCFP), green (eGFP), and yellow (eYFP) fluorescent proteins at λ_{max} =860, 920 and 960 nm, respectively, all fall into the tuning range of a standard Ti:sapphire laser equipped with broadband optics. The absolute values of the two-photon action cross-section, σ_{TPE} , at the maxima vary between 8 and 40 GM ($1 \text{ GM} = 10^{-50} \text{ cm}^4\text{s}^{-1}\text{photon}^{-1}$). The limited tuning range of our standard Ti:sapphire system did not allow for the identification of the maximum of the two-photon spectrum for DsRed, predicted to be around 1100 nm. The highest value obtained for DsRed was 20 GM at the wavelength of 980 nm.

It should be noted that the spectra and absolute values of the TPE action cross-sections reported here on eGFP are in good agreement with the values previously reported[3], and that of eYFP closely resembles the results obtained for a non-commercial, improved YFP mutant Citrine[18]. For the most redshifted autofluorescent protein, DsRed, current data suggest that it forms tetrameric complexes even at low concentrations[19] which, in turn, renders the definition of a molar absorption ϵ and thus the actual concentration in our experiment difficult[18, 20]. For the data presented the values of ϵ given by the manufacturer were used (table 2.1)[6, 21].

The increase of the TPE action cross-section at wavelengths below 760 nm, for which a sub-quadratic power dependence ($\alpha = 1.68 \pm 0.12$) was found, does not correspond to any increase in the one-photon spectrum below 380nm. This new component has recently been described by Marchant et al. [22] as an irreversible “greening” of the protein by a three-photon



transformation process, which might also explain the deviation from the expected quadric power dependence. Such higher order photobleaching processes have been established before for a variety of other fluorophores[23].

Figure 2.2 is subsequently used for a quantitative comparison of the one-photon (solid lines, top wavelength axis) with the two-photon absorption cross-section spectra (points, bottom wavelength axis). The two-photon spectra roughly follow the shape of the one-photon spectra (when dividing the wavelength scale by two). However, a significant blue-shift in excitation is observed recurrently for the two-photon excitation spectra in comparison to the one-photon spectra[2, 16]. Whereas the absorption spectra are shifted, the fluorescence emission spectra stay unchanged for one and two photon excitation[24, 25], as predicted from Kasha's rule.

The blue-shift in the absorption spectrum is probably due to an additional, low-symmetry vibrational mode which couples to the electronic transition in order to get sufficient oscillator strength for the two-photon absorption process. For the pure electronic (0-0)-transition the two-photon absorption process is parity-forbidden. We quantified the blue shift for the autofluorescent proteins by a least-square fit which overlays the one- and the two-photon spectra. The values for the blue-shift found in this way are 255, 773 and 1290 cm^{-1} for eCFP, eGFP and eYFP, respectively.

It is interesting to note that vibrational modes of 222, 775 and 1507 cm^{-1} have been identified for wild-type GFP by low-temperature line-narrowing experiments[26]. The different shifts found for the various autofluorescent proteins point to the appealing conclusion that depending on the fluorophore a different vibrational mode couples to the two-photon excitation process. However, it can not be excluded likewise that the different shifts

are mediated by a change in the protein environment.

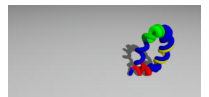
The absolute TPE action cross-sections as determined for the autofluorescent proteins (figure 2.2) and the flavine mononucleotide (figure 2.3) determined here are used to quantify the relative detection yield of the autofluorescent proteins in comparison to flavines necessary for single-molecule studies in living mammalian cells.

Following a strategy developed by Harms et al. [11] we define the excitation-wavelength dependent relative detection yield for the autofluorescence proteins as:

$$R_{(OPE/TPE)} = \frac{\eta}{\eta_{flavine}} \cdot \frac{\sigma(\lambda)}{\sigma_{flavine}(\lambda)} \quad (2.2)$$

where the experimental detection efficiencies for the various fluorophores, η , and the absorption cross-sections, σ_{OPE} and σ_{TPE} , for the one- or two-photon case are considered. In the case of two-photon excitation $\eta/\eta_{flavine}$ was close to unity. The values for one- and two-photon excitation are summarized in table 2.2. In the one-photon case the low values of relative detection yield for eCFP and eGFP ($R_{OPE} < 10$) render their use for wide-field single-molecule studies in cells extremely difficult. For eYFP and DsRed ($R_{OPE} > 100$) single-molecule studies have been demonstrated[11].

This picture significantly changes for two-photon excitation. Indeed, due to the super-linear scaling of the two-photon absorption cross-section with the one-photon absorption cross-section (table 2.1), the relative detection yield for all autofluorescent proteins becomes $R_{TPE} > 35$. Such high relative detection yield leads to the extremely low autofluorescent background compulsory for single-molecules studies in life cells. Preliminary data from our laboratory show that the autofluorescent background is indeed largely (by a factor of ten or higher) reduced with respect to the



autofluorescent background in one photon measurements.

2.5 Conclusions

We have shown that the use of two-photon excitation does largely enhance the detection ratio of all autofluorescent proteins against the autofluorescence background expected from flavines in living cells. The higher detectability is the result of the super-linear scaling between the one- and two-photon absorption cross-sections which has been previously reported for organic fluorophores. The presentation of the two-photon spectra allows one to optimize the excitation wavelength for any particular experiment including those in which one strives to use fluorescence resonant energy transfer between the various autofluorescent proteins[9, 10].

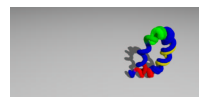
In conclusion, it should be mentioned that we have neglected the effect of photobleaching in our discussion, which is another factor important for single-molecule studies[11]. It has been generally found that the process of photobleaching is enhanced (typically by one order of magnitude) for two-photon excitation with respect to one-photon excitation[23, 24, 27] (see also figure 2.4). This further expands the enhancement of detectability due to the favorable spectroscopic properties investigated here. Further studies of the photobleaching behavior dependence on the pulse width and wavelength, for example, will be needed to finally decide if two-photon excitation will be superior to one-photon excitation for single-molecule studies in cells.

2.6 Acknowledgement

This work was supported by funds from the Dutch ALW/FOM/NWO program for Physical Biology (99FBK03). L.C. acknowledges support from DGA/DSP (France) and the European Marie-Curie fellowship program (IHP-MCFI-1999-00736).

fluorophore	one-photon excitation		two-photon excitation		
	λ (nm)	σ_{OPE} (10^{-16} cm ²)	λ (nm)	σ_{TPE} (GM)	shift (cm ⁻¹)
eCFP	434	0.99	860	7.87	255
eGFP	489	2.10	920	41.21	773
eYFP	514	3.21	960	24.98	1290
DsRed	558	0.86	960	11.01	n.d.
FMN	266	1.22[30]	-	0.39	n.d.
	373	0.40	760		
	445	0.48	-		

Table 2.1: Maximal values of the one-photon absorption (σ_{OPE} , and the TPE action cross-sections (σ_{TPE} ; 1GM = 10^{-50} cm⁴ s/ photon) of the commercial autofluorescent proteins and of flavine mononucleotide (FMN). Blue-shift of the two-photon spectra with the respect to the one-photon spectra.



fluorophore	one photon		two photon	
	λ (nm)	R_{OPE}	λ (nm)	R_{TPE}
eCFP	435 [†]	3.4	860	36
	457 [‡]	1.8		
eGFP	488 ^{†,‡}	8.7	920	467
eYFP	514 ^{†,‡}	405	960	566
dsRed	532 [‡]	$> 10^4$	960	251

Table 2.2: Relative detection-ratio of the autofluorescent proteins versus flavine mononucleotide for one- (R_{OPE}) and two-photon excitation (R_{TPE}). Values of R_{OPE} were taken from Harms et al. [11]. The value of R_{TPE} for DsRed will be considerably higher for its maximum absorption at wavelengths above 1000 nm.

([†]: values for excitation at the peak absorption; [‡]: values for wavelengths associated with the commonly used laser lines)

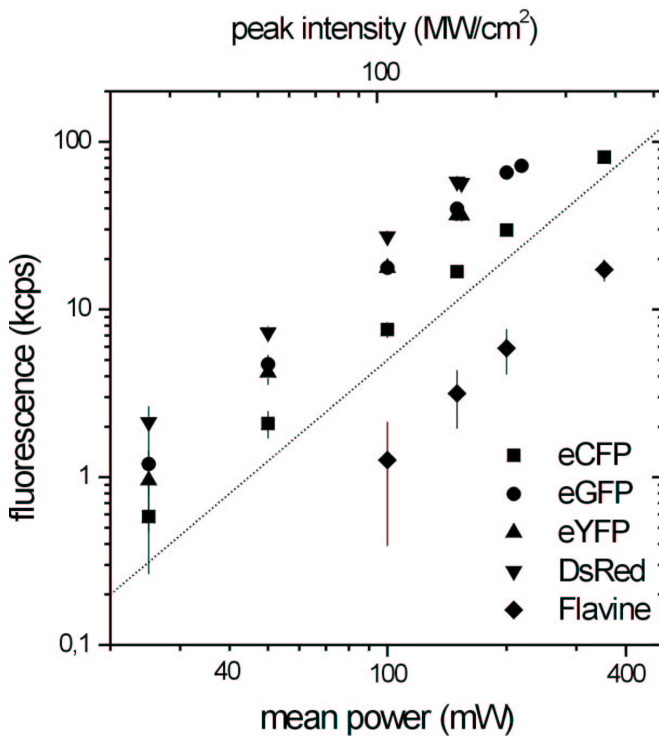
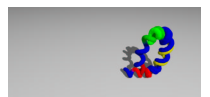


Fig.1

Figure 2.1: Dependence of the fluorescence signal on the excitation intensity for the autofluorescent proteins at their peak two-photon absorption wavelength; eCFP: 860 nm, eGFP: 920 nm, eYFP: 960 nm, DsRed: 980nm, and flavine mononucleotide: 760nm. The fluorescence follows a power-law dependence on the intensity with a mean exponent of 2.00 ± 0.03 (dotted line).



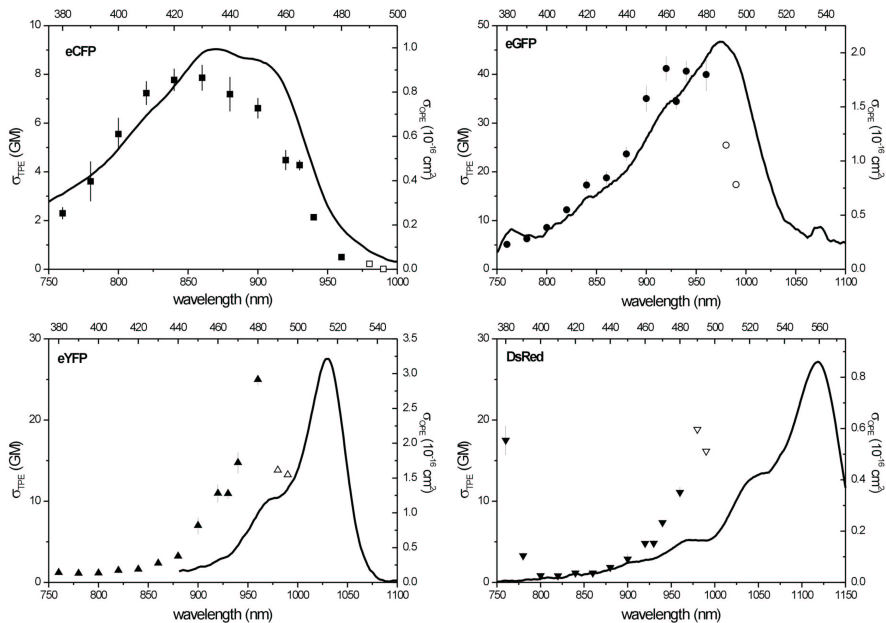


Figure 2.2: Absolute TPE action cross-sections (σ_{TPE} , left axes) of eCFP, eGFP, eYFP, and DsRed in phosphate buffer (wavelength scale bottom). The values for $\lambda \leq 960$ nm were calibrated against the values for fluoresceine ($pH > 11$)[16] (filled symbols). For $\lambda > 960$ nm the calibration for 960 nm was extrapolated. The one-photon absorption cross-sections (σ_{OPE} , right axes) are shown for comparison (solid lines; wavelength scale top).

Fig.3

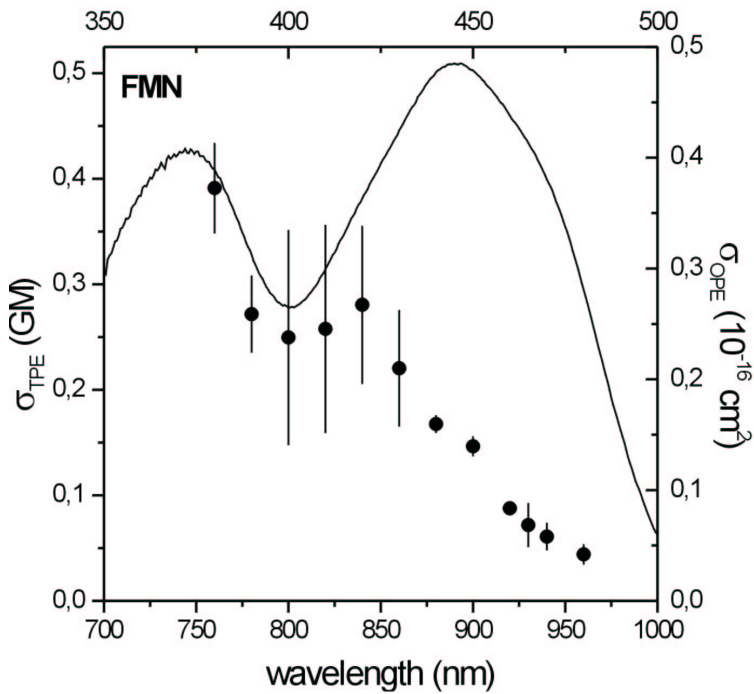
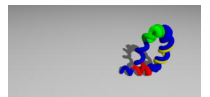


Figure 2.3: Absolute TPE action cross-sections (σ_{TPE} , left axis) of flavine mononucleotides in phosphate buffer (symbols). The one-photon absorption cross-section (σ_{OPE} , right axis) is shown for comparison (solid line; wavelength scale top).



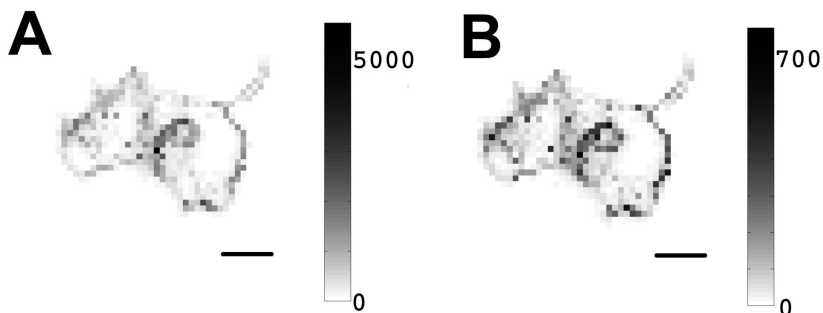


Figure 2.4: Two consecutive confocal images of tsa201 cells transfected with membrane-anchored eGFP (eGFP-C10HRas[28]). The images were taken with 5 ms illumination of 1.5 mW, 940 nm laser. The signal is comparable to the signal of this type of cell under one-photon illumination. About 90% of the fluorescence in the first image (**A**) is bleached after only one exposure (**B**). The bleaching is more than one order of magnitude faster than in the one-photon case[11].

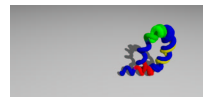
As two-photon photobleaching is reported to depend on the third order [23] or even fourth order[29] of the excitation intensity, one would have to resort to long integration times ($\gg 5$ ms) and low excitation intensity to be able to repeatedly image single molecules. This approach, however, does not allow for the study of dynamics inside the cell below the timescale of a few seconds.

Due to the limited intensity range used in preliminary measurements with spincoated Rhodamine we did not observe higher order bleaching as reported by other groups.[23, 29]

The scale bar is $10\mu\text{m}$.

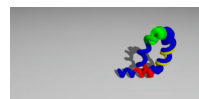
Bibliography

- [1] GA Blab, PHM Lommerse, L Cognet, GS Harms, and T Schmidt. Two-photon excitation action cross section of the autofluorescent proteins. *Chemical Physics Letters*, 350:71–77, 2001.
- [2] W Denk, DW Piston, and WW Webb. *Handbook Of Biological Confocal Microscopy*, pages 445–457. Plenum Press, 1995.
- [3] C Xu, W Zipfel, JB Shear, RM Williams, and WW Webb. Multiphoton fluorescence excitation: new spectral windows for biological nonlinear microscopy. *PNAS (USA)*, 93(20):10763–10768, 1996.
- [4] O Shimomura, F Johnson, and Y Saiga. Extraction, purification and properties of aequorin, a bioluminescent protein from the luminous hydromedusan aequorea. *J. Cell. Comp. Physiol.*, 59:223–239, 1962.
- [5] RY Tsien. The green fluorescent protein. *Annu. Rev. Biochem.*, 67, 1998.
- [6] MV Matz, AF Fradkov, Labas YA, AP Savitsky, AG Zaraisky, ML Markelov, and SA Lukyanov. Fluorescent proteins from nonbioluminescent anthozoa species. *Nature Biotechnology*, 17:969–973, 1999.
- [7] A Mallavarapu, K Sawin, and T Mitchison. A switch in microtubule dynamics at the onset of anaphase b in the mitotic spindle of *Schizosaccharomyces pombe*. *Current Biology*, 9:1423–1426, 1999.
- [8] R Iino, I Koyama, and A Kusumi. Single molecule imaging of green fluorescent proteins in living cells: E-cadherin forms oligomers on the free cell surface. *Biophysical Journal*, 80:2667–2677, 2001.
- [9] VA Romoser, PM Hinkle, and A Persechini. Detection in living cells of Ca^{2+} -dependent changes in the fluorescence emission of an indicator composed of two green fluorescent proteins linked by a calmodulin-binding sequence. a new class of fluorescent indicators. *Journal of Biological Chemistry*, 272:13270–13274, 1997.
- [10] A Miyawaki, J Llopis, R Heim, JM McCaffery, Adams JA, M Ikura, and RY Tsien. Fluorescent indicators for Ca^{2+} based on green fluorescent proteins and calmodulin. *Nature*, 388:882–887, 1997.



- [11] GS Harms, L Cognet, PHM Lommerse, GA Blab, and T Schmidt. Autofluorescent proteins in single-molecule research: Applications to live cell imaging microscopy. *Biophysical Journal*, 80:2396–2408, 2001.
- [12] GS Harms, L Cognet, PHM Lommerse, GA Blab, H Kahr, HP Spaink, C Romanin, and T Schmidt. Imaging of L-type Ca^{2+} channels in live cells. *Biophysical Journal*, 81:2639–2646, 2001.
- [13] RC Benson, RA Meyer, ME Zaruba, and GM McKhann. Cellular autofluorescence – is it due to flavins? *Journal of Histochemistry and Cytochemistry*, 27:44–48, 1979.
- [14] C Bubeck, A Grund, A Kaltbeizel, D Neder, A Mathy, and G Wegner. *Organic Molecules for Nonlinear Optics and Photonics*, pages 335–343. Kluwer Academic Publishing, 1991.
- [15] C Xu and WW Webb. Measurement of two-photon excitation cross sections of molecular fluorophores with data from 690 to 1050 nm. *J. Opt. Soc. Am. B*, 13:481–491, 1996.
- [16] MA Albota, C Xu, and WW Webb. Two-photon fluorescence excitation cross sections of biomolecular probes. *Applied Optics*, 37:7352–7356, 1998.
- [17] M Göppert-Mayer. Über Elementarakte mit zwei Quantensprüngen. *Annalen der Physik*, 9:273–295, 1931.
- [18] AA Heikal, ST Hess, GS Baird, RY Tsien, and WW Webb. Molecular spectroscopy and dynamics of intrinsically fluorescent proteins: coral red (dsred) and yellow (citrine). *PNAS (USA)*, 97:11996–12001, 2000.
- [19] GS Baird, DA Zacharias, and RY Tsien. Biochemistry, mutagenesis, and oligomerization of dsred, a red fluorescent protein from coral. *PNAS (USA)*, 97:11984–11989, 2000.
- [20] LA Gross, GS Baird, RC Hoffman, KK Baldrige, and Tsien RY. The structure of the chromophore within dsred, a red fluorescent protein from coral. *PNAS (USA)*, 97:11990–11995, 2000.
- [21] *Living ColorsTM Red Fluorescent Protein*. Clontech, 1999.
- [22] JS Marchant, GE Stutzmann, MA Leissring, FM LaFerla, and

- I Parker. Multiphoton-evoked color change of dsred as an optical high-lighter for cellular and subcellular labeling. *Nature Biotechnology*, 19: 645–649, 2001.
- [23] GH Patterson and DW Piston. Photobleaching in two-photon excitation microscopy. *Biophysical Journal*, 78:2159–2162, 2000.
- [24] EJ Sánchez, L Novotny, GR Holtom, and XS Xie. Room-temperature fluorescence imaging and spectroscopy of single molecules by two-photon excitation. *Journal of Physical Chemistry A*, 101:7019–7023, 1997.
- [25] A Volkmer, V Subramaniam, DJ Brich, and Jovin TM. One- and two-photon excited fluorescence lifetimes and anisotropy decays of green fluorescent proteins. *Biophysical Journal*, 78:1589–1598, 2000.
- [26] TMH Creemers, AJ Lock, V Subramaniam, TM Jovin, and S Völker. Three photoconvertible forms of green fluorescent protein identified by spectral hole-burning. *Nature Structural Biology*, 6:557–560, 1999.
- [27] M Sonnleitner, GJ Schütz, and T Schmidt. Imaging individual molecules by two-photon excitation. *Chemical Physics Letters*, 300: 221–226, 1999.
- [28] PHM Lommerse, GA Blab, L Cognet, GS Harms, BE Snaar-Jagalska, HP SPaink, and T Schmidt. Single-molecule imaging of the h-ras membrane-anchor reveals domains in the cytoplasmic leaflet of the cell membrane. *Biophysical Journal*, in press, 2004.
- [29] T-S Chen, S-Q Zeng, Q-M Luo, Z-H Zhang, and W Zhou. High-order photobleaching of green fluorescent protein inside live cells in two-photon excitation microscopy. *Biochemical and Biophysical Research Communications*, 291:1272–1275, 2002.
- [30] J Koziol. Fluorometric analyses of riboflavin and its coenzymes. *Methods of Enzymology*, 18B:253–285, 1971.



This page intentionally contains only this sentence.

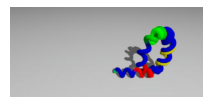
Chapter 3

Aggregation of the β_2 Adrenergic Receptor Studied on the Level of Individual Receptors

The work described in this chapter will be published as “Single molecule studies of the β_2 adrenergic receptor reveal aggregation before stimulation”. [1]

3.1 Abstract

We present a study of the oligomerization of β_2 adrenergic receptors (β_2 ARs) upon stimulation with an agonist on live human cells. Using highly sensi-



tive microscopy techniques we follow individual eYFP-tagged β_2 AR (β_2 AR-eYFP) molecules over time in the plasma membrane. Our data shows that the β_2 AR-eYFP is constitutively expressed as oligomers ($N \leq 2$) and that further oligomerization ($N > 3$) of the receptor is induced within seconds after agonist stimulation.

3.2 Introduction

Guanidine nucleotide binding protein (G protein)-coupled receptors are encoded by the fourth largest gene family in man and play an important role in the transduction of extracellular signals across the plasma membrane of cells by the recognition and binding of specific ligands, such as ions, transmitters, and peptides, or – in the case of rhodopsin – by absorption of photons, upon which intracellular G proteins are activated. As such, these receptors mediate a variety of physiological functions, including vision, taste and olfaction, cognition, and immune regulation[2]. Until recently, GPCRs were thought to act as monomeric transmembrane entities. Accumulating evidence, however, now suggests GPCRs to exist in monomeric, dimeric, and various other oligomeric forms[3].

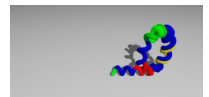
The β_2 adrenergic receptor (β_2 AR) is an important and well-characterized target for pharmaceutical drug development efforts as ligands for this receptor are successfully used for the treatment of a variety of conditions. The cloning of the β_2 AR gene showed that the β_2 AR and rhodopsin are members of a gene family that share sequence homology and a presumed "seven membrane spanning" topography[4]. A great number of receptors have been identified, and β_2 adrenergic receptors have become the proto-

type for the intense study of GPCRs, which has led to the unraveling of the structural basis of receptor function[5].

To date several techniques have been employed to study the dimerization of β_2 ARs [6–8], including the immunoblotting upon immunoprecipitation [7, 9–11], the functional rescue by complementation of constitutively desensitized mutant receptors [12], computational methods [13], and a variety of fluorescent methods[9, 14–20]. GPCRs, including β_2 ARs, have for instance been linked to fluorescent proteins with different fluorescence properties, such as the different fluorescent forms of the Green Fluorescent Protein (GFP) from *Aequorea victoria*, to allow the measurement of fluorescence resonance energy transfer (FRET) when two GPCRs are in close enough proximity [9, 14–17].

A widely used modification of this approach is bioluminescence resonance energy transfer (BRET) which has developed in recent years as a new technique to study protein-protein interactions. Protein partners of interest are tagged with either Renilla luciferase or green fluorescent protein (GFP). Non-radiative energy transfer between the excited luciferase and the GFP permits the study of spatial relationships between the two partners [9, 14, 18–20].

To investigate the potential oligomerization of the β_2 ARs in real time we employed a highly sensitive microscopy method that allows the imaging and localization of individual eYFP-tagged β_2 ARs in real time. Our studies show the β_2 AR to be predominantly expressed as a dimeric receptor but the β_2 AR is also constitutively present in the form of higher order multimers. Moreover, the β_2 AR agonist isoproterenol modulates the relative ratios between the dimeric and multimeric forms of the β_2 AR.



3.3 Experimental Section

3.3.1 Single Molecule Microscopy

The experimental setup has been described in detail previously [21, 22]. In short, HEK 293 cells were mounted onto an inverted microscope (Zeiss Axiovert100). The temperature was controlled by a stabilized water flow system and set to 37°C.

The sample was illuminated for 3 ms with the 514 nm line from an Ar⁺-laser (Spectra Physics), and imaged through a high aperture, 100× oil-immersion objective (Zeiss, NA = 1.4). The excitation light was suppressed in the detection path by use of a filter combination appropriate for eYFP (DCLP 530, HQ570/80, Chroma Technology; OG530, Schott). A 150 mm achromatic lens formed the image on a back-illuminated, liquid-nitrogen-cooled CCD camera (400 × 1340 pixels, 20 × 20 μm^2 pixel size, LN/CCD-400-PB, Princeton Instruments). The total collection efficiency of the setup was better than 7%.

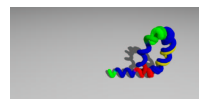
The camera was used in kinetic mode, resulting in sets of 10 images with a lag time of 5 ms between images. Each image was analyzed for single molecule signatures as described in detail previously[22]. In short threshold defined positions in the images were fitted with a Gaussian distribution, yielding positional information with 50 nm accuracy and the signal intensity with a precision of $\approx 20\%$, limited by shot-noise and the readout-noise of the CCD-camera.

3.3.2 Cell Preparation

HEK 293 cells were cultured in DMEM medium supplemented with streptomycin (100 μ g/ml), penicillin (100 U/ml), and 10% bovine serum in a humidified atmosphere (95%) at 5% CO₂ and 37°C. The cells were transferred every 4 days. To obtain expression of the β_2 AR-eYFP fusion protein at the desired level, cells exhibiting confluence of approximately 50% were transfected with 1 μ g of cDNA and 3 μ l FUGENE-6 (Roche Biochemicals) six days prior to measurement. The cDNA was a gift from Dr. G. Milligan (Glasgow, UK), the construction of the receptor plasmide is described in Ramsay et al. [20]. Cells were separated and reseeded onto sterile 25 mm #1 microscope glass slides two days before measurement. The overall transfection efficiency was in the range of 30-50%. For measurements, cells were gently washed thrice with phosphate-buffered saline (PBS, 150 mM NaCl, 10 mM Na₂HPO₄, pH 7.4) before imaging in this buffer.

3.3.3 Stimulation Assays

For stimulation assays, cells exhibiting a low level of fluorescence were selected by eye and imaged as described above. After pipetting 5 μ l of 1 mM stock solution of either the agonist (-)isoproterenol or its biologically inactive isoform (+)isoproterenol (both: Sigma-Aldrich chemicals) into the cell-bath, cells were imaged for another 10 minutes. Due to the addition of liquid some refocusing was necessary, adding a delay of 1 minute between the images of unstimulated and stimulated cells.



3.3.4 Computer Simulations

Simulated intensity distributions were generated using Matlab (MathWorks, Inc.). Oligomers were considered to consist of N independent fluorophores with a normally distributed intensity of 200 counts ($\sigma = 40$), each with a mean bleaching time of 1.5 images (4.5 ms) and a recovery probability of 1%, consistent with values published by Harms et al. [23]. The intensities of the active fluorophores were then combined into one peak, was placed into an image with a noise level of 6 counts per pixel (rms) and fitted with the same parameters as the measured data to ensure that possible influence of the fitting procedure would not affect the results.

The simulation of an oligomer ended when all N fluorophores were bleached.

3.3.5 Stoichiometric Analysis

Probability density functions (PDF, $\rho(I)$) of measured and simulated data were fit to a model distribution using a non-linear least-square algorithm. The model distribution is derived from a “single molecule footprint” obtained by measurements of a membrane anchored eYFP moiety (hRAS-eYFP) expressed in mammalian cells.

The model allows for a shift in the peak intensity (maximum of the PDF) and generates oligomer distributions by convolution, $\rho_{i+1}(I) = \rho_i(I) \otimes \rho_1(I) = \int dx \rho_i(x) \cdot \rho_1(I-x)$ (“monomer-dimer-fit”, figure 3.3 and table 3.1). The full distribution for N -oligomers, $\rho_{total}(I) = \sum_N \alpha_i \cdot \rho_i(I)$, $\sum_N \alpha_i = 1$, is fully described by the monomeric distribution and the relative populations α_i .

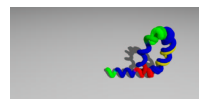
3.4 Results and Discussion

Heterologous expression of genes by standard transfection techniques generally results in the over-expression of the protein of interest. While this is of advantage for various biochemical assays, as it provides more material to be analyzed, it may also increase the probability of artifacts caused by the unphysiologically high density of the protein.

In contrast, highly sensitive analytical methods, such as single-molecule fluorescence microscopy, require low levels of protein expression, i.e. a low density of fluorophores. Transient expression of the β_2 AR-eYFP in HEK 293 cells typically yields a receptor expression level of $> 10^4$ β_2 AR molecules/cell, as can be determined by the fluorescence intensity of transfected cells (figure 3.1B). This number is two orders of magnitude above the single-molecule detection-limit of ≈ 1 fluorophore/ μm^2 . We have previously used photobleaching to reduce excessive fluorophores before the measurement of single molecules [24]. However, this approach was considered not useful for the detection of receptor oligomers.

It is characteristic for transient transfection that, after an initial rise, the receptor-expression in transfected cells will diminish over time. For transiently transfected HEK 293 cells expressing the β_2 AR we found that 6 days after transfection of the cells the average density of fluorophores on the cell membrane had dropped to a level where individual fluorophores can be identified (figure 3.1C). This low density ($\leq 0.3 \mu\text{m}^{-2} = 0.013$ per pixel) also assures that the probability to find two receptors in close proximity purely by coincidence is less than 1%.

In order to analyze the local stoichiometry of the β_2 AR we also had



to establish a “single molecule footprint” for monomeric eYFP in a mammalian cell line. We did this using the membrane anchored hRAS-eYFP[25] under the same expression conditions described above for the β_2 AR (figure 3.2, squares). This footprint was subsequently used for analysis as described in section 3.3.5. The intensity distribution of monomeric eYFP molecules that we obtained in HEK 293 cells is essentially identical to one measured for eYFP in artificial membranes or in gels[23].

The intensity distribution of β_2 AR-eYFP deviates markedly from the intensity distribution we obtained for monomeric eYFP, indicating that against our predictions at least a part of β_2 AR-eYFP are present as oligomers in cells at rest (figure 3.2, circles).

A further, dramatic change in the intensity distribution of β_2 AR-eYFP is observed upon stimulation of the receptors with the β_2 AR agonist (-)isoproterenol (figure 3.2, Δ). Analysis of the data indicates, in agreement with previous reports[14], that the β_2 AR agonist promotes the aggregation of β_2 AR-eYFP.

A change in stoichiometry can be quantified by a fit of the PDF according to a “monomer-dimer” model, in which one computes the expected di-, tri-, N -mer distributions by repeated convolution of the monomer distribution.

A more careful analysis of the data, however, shows that the intensity distribution obtained for the β_2 AR can not be fully explained by the simple assumption that the previously mainly monomeric receptor now forms dimers. On the one hand, even before stimulation the intensity distribution deviates from the “single-molecule footprint”. On the other hand, a fit according to the “monomer-dimer” model described previously reveals that

the intensity distributions are broader and show less pronounced features than expected (figure 3.3), especially in the case of the stimulated β_2 AR.

The cause for this deviation is the particular bleaching and blinking properties of eYFP[26, 27], which we used as fluorophore for our experiments.

As the case of the negative control with (+)isoproterenol clearly shows, every population of oligomers will eventually bleach, leading to a strong monomer-like peak. In the case of both (+) and (-)isoproterenol stimulation, the cells were imaged before and after addition of the substance. Therefore the stimulated β_2 AR-eYFP are expected to exhibit stronger effects of photobleaching.

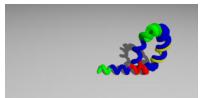
This also means that the fitting method will severely underestimate the actual number and size of oligomers present. Photobleaching continuously removes fluorophores during the measurement, and in the case of stimulated cells, even before the measurement.

The number of fluorophores bleached is calculated by using the probability $P(t) = \int_0^T \frac{1}{\tau} e^{-\frac{t}{\tau}} dt$ that a fluorophore with bleaching constant τ will be bleached after time t . For N independent fluorophores in an aggregate, the chance that n of those are bleached is given by the binomial distribution

$$B_p^N(n) = \binom{N}{n} p^n (1-p)^{N-n} \quad (3.1)$$

where $p = P(t_{exposure})$ denotes the probability for each fluorophore to bleach during the exposure. After the i^{th} exposure, the distribution is given by $B_{p_i}^N(n)$, with $p_i = 1 - (1-p)^i$.

As the bleaching is photoinduced, it will occur during acquisition of the image, thereby further broadening the distribution. To complicate matters



further, eYFP is known to exhibit blinking on the millisecond timescale, in which case one can not only identify stepwise reduction of signal of an aggregate of receptors, but with a small probability also the stepwise return of the signal.

To assess the influence of these photophysical characteristics of eYFP, we chose to simulate the behavior of N -mers with the same properties as found in eYFP[24] and compute the resulting PDFs. The curves in figure 3.4 have to be considered as an extreme case, in which an N -mer is followed until all fluorophores are bleached. Under this assumption it is generally not possible to clearly resolve the N peaks in the distribution which correspond to the consecutive bleaching of the constituent fluorophores.

The fitting of these simulation results, presented in table 3.1, shows that rapid photobleaching – while causing a severe under-estimation of the oligomerisation state – still permits to follow and distinguish changes in intensity caused by aggregation.

The qualitative shift in the intensity distribution observed after stimulation with (-)isoproterenol (figure 3.2) was quantified using the simulation results. The ratio of monomer/dimer of 81%/19% observed before stimulation are close to those found for dimers in the simulation, leading to the assumption that the β_2AR forms mainly dimers if expressed in a mammalian cell system. After stimulation with its agonist, and despite photo-bleaching, the distribution shifts markedly towards higher intensities (78%/14%/8% for mono-, di- and trimers, respectively), indicating the formation of aggregates with $N \geq 4$. The bleaching of such an aggregate with $N = 4$ is shown in figure 3.5.

In the control, a stimulation with the biologically inactive stereoisomer

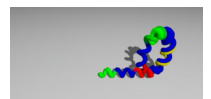
(+)isoproterenol, the intensity distribution returns almost to the monomer distribution (7% dimer). As all stimulation experiments are conducted after taking images of the unstimulated cells, this shift was attributed to photo-bleaching as opposed to a reaction of the receptor.

3.5 Conclusions

We have shown that β_2 ARs are constitutively expressed as oligomeric structures, mainly monomers and dimers when transiently expressed at low level in human cells. Stimulation of β_2 AR expressing cells with the β_2 AR agonist isoproterenol increases the size of these β_2 AR oligomers from dimers to aggregates with $N \geq 4$.

This change in aggregate size is a clear reaction of the receptor to stimulation with an agonist. While we cannot rule out completely that the aggregation is caused – at least in part – by the downregulation of the receptor, our data does not show evidence for internalization. In contrast, the biologically inactive stereoisomer of isoproterenol does not modulate β_2 AR oligomerization, as only bleaching of the eYFP fluorophore is observed, indicating that stimulation and aggregation are functionally linked.

In consequence we were also able to show that eYFP can be used as a marker to study aggregation of membrane proteins *in vivo*, despite its rapid photobleaching, which can interfere with the interpretation of the data if not properly taken into account. Furthermore we find a tentative link between the dimerization of GPCRs and their biological function in the surprising discovery that a biologically inactive hH1-GPCR occurs in monomeric form if expressed in HEK 293 cells..

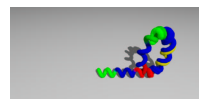


3.6 Acknowledgment

The β_2 -receptor-eYFP fusion protein was a gift from Dr. G. Milligan (Glasgow, UK).

		monomer-dimer fit
β_2 AR unstimulated	monomer	81%
	dimer	19%
	trimer	-
β_2 AR stimulated (-)-isoproterenol	monomer	78%
	dimer	14%
	trimer	8%
β_2 AR stimulated (+)-isoproterenol	monomer	93%
	dimer	7%
simulation dimer	monomer	91%
	dimer	9%
simulation trimer	monomer	43%
	dimer	57%
	trimer	< 1%
simulation tetramer	monomer	26%
	dimer	38%
	trimer	34%
	tetramer	< 1%

Table 3.1: Results from fitting the intensity distributions of β_2 AR before and after stimulation. While in any case addition of the agonist causes a shift from the monomer population into higher aggregation states. Simulations have been performed to see how the photobleaching affects this distribution. See section 3.3.5 on page 56 for more information on the model used for fitting.



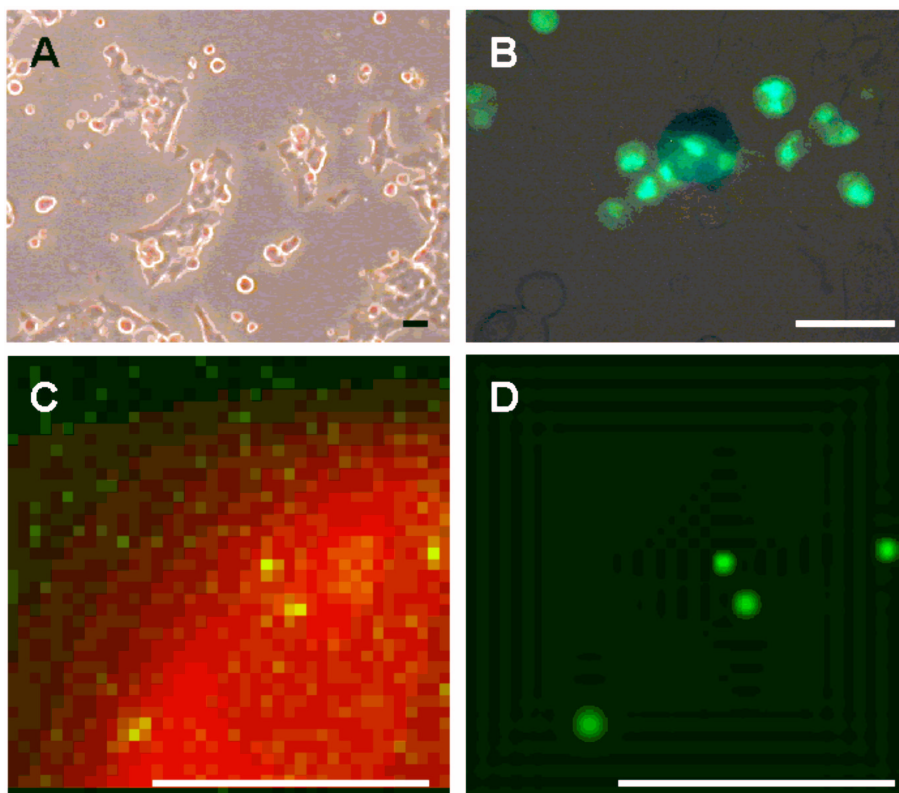


Figure 3.1: HEK 293 cells were grown in culture (**A**, white-light image); 24 hours after transfection the cells exhibited strong fluorescence (**B**, $> 10^4$ fluorescent molecules per cell). The transfection efficiency was roughly 30%. The number of fluorescent molecules decreases over time to a level where single fluorophores can be separated (**C**, 6 days after transfection). Using a fitting procedure as described in the text, one can obtain positions and intensities of individual molecules (**D**). The scalebars are $5\mu\text{m}$.

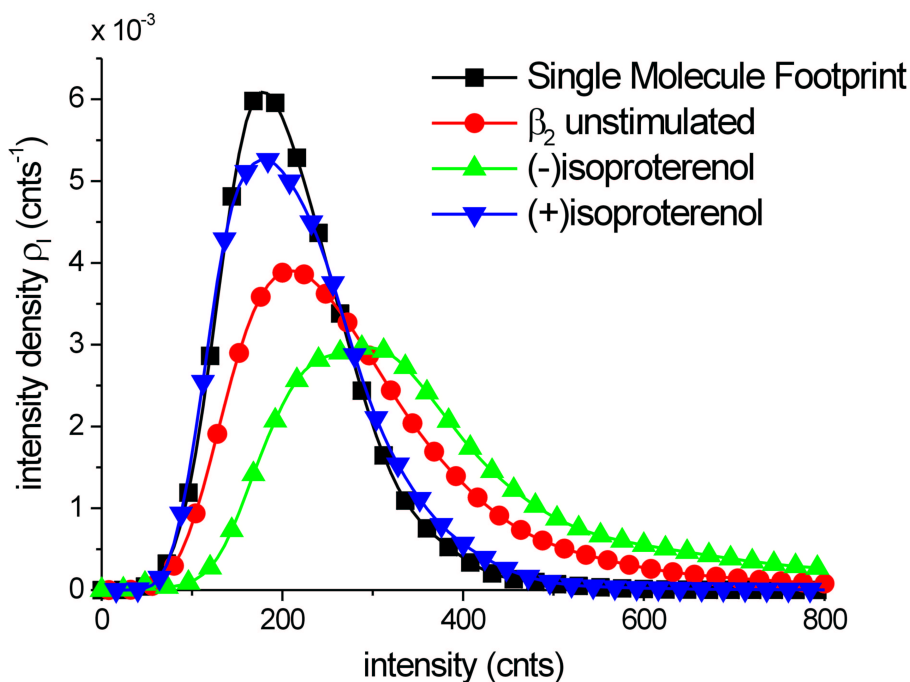
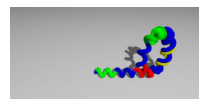


Figure 3.2: Intensity distribution of individual β_2 AR aggregates in HEK 293 cells. The “single molecule footprint” for monomeric eYFP has been obtained by an inactive GPCR-eYFP construct imaged under the same conditions. Even before stimulation, the intensities recorded for β_2 AR show a clear deviation from the monomer distribution. Upon stimulation with the agonist (-)isoproterenol a marked shift towards higher intensities and therefore higher aggregation is observed. Addition of the inactive isoform (+)isoproterenol exhibits no such effect. The lower intensities found in this case are most likely an effect of photobleaching.



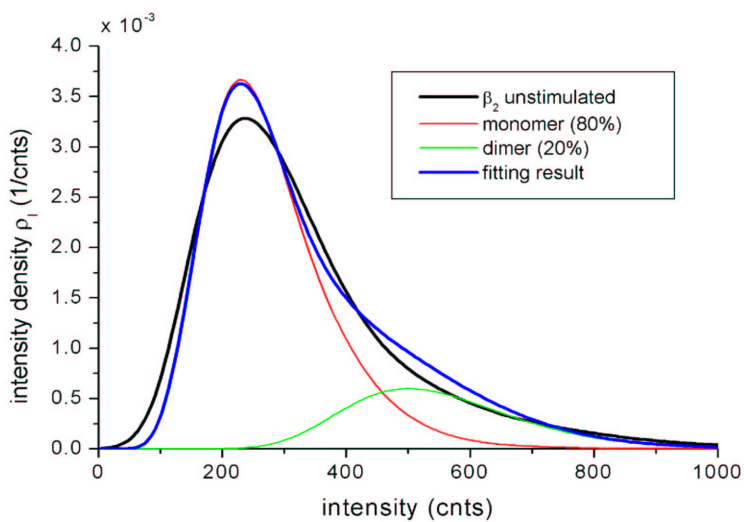


Figure 3.3: Example of the fit of individual β_2AR in HEK 293 cells before stimulation. The experimental distribution is wider than the single eYFP “footprint” found for monomeric eYFP in mammalian cells. This widening can be explained by the presence of dimers and the effect of photobleaching.

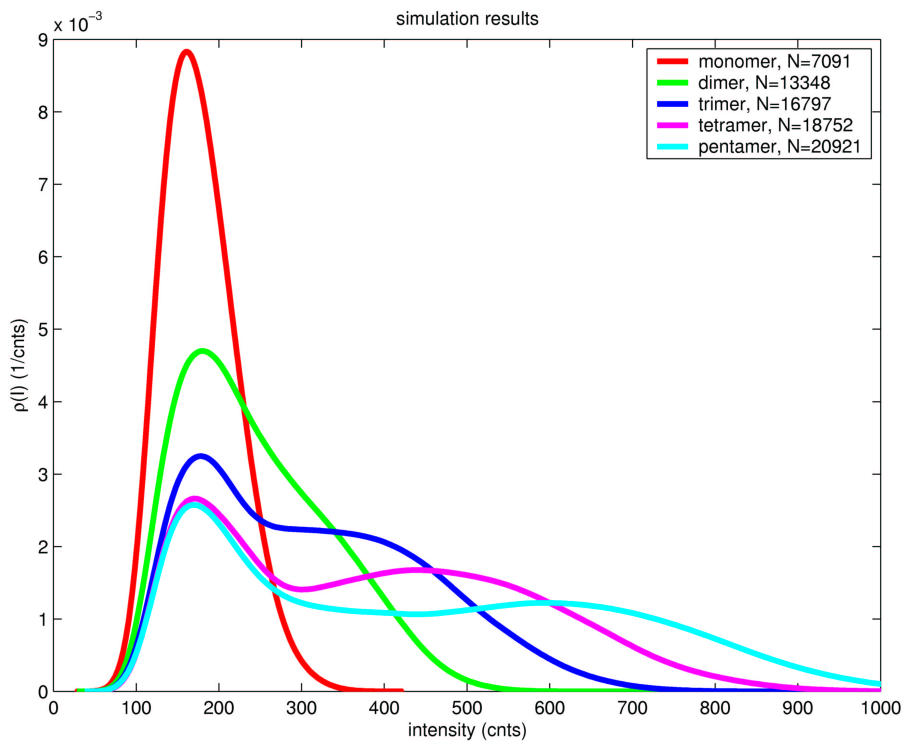
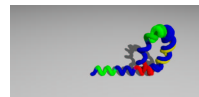


Figure 3.4: Intensity distribution simulation of purely mono-, di-, tri-, tetra-, and pentameric fluorescence complexes. The mean bleaching and recovery times were chosen to match those of eYFP[24]. See section 3.3.4 on page 56 for details on the simulation.



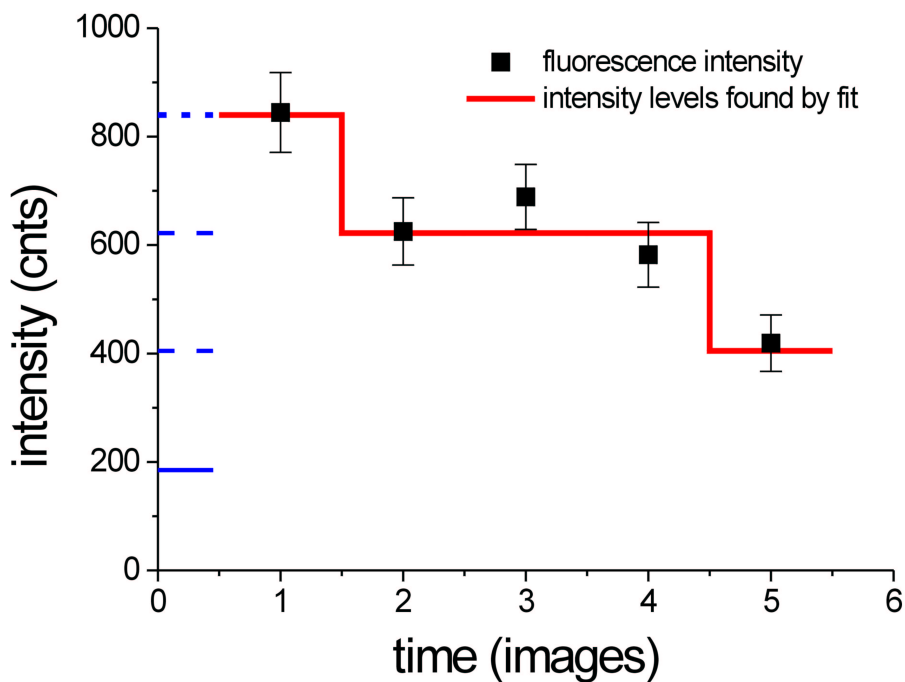
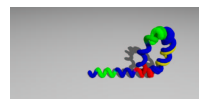


Figure 3.5: A multistep photobleaching events for β_2AR after stimulation with (-)-isoproterenol ($N = 4$, symbols) is described well by the intensity levels found in a fitting of the PDF. The levels (lines) of intensity are not evenly spaced due to the asymmetry of the monomer intensity distribution. The event occurred at the end of a kinetic-mode-cycle, therefore the drop to monomeric level and eventual complete bleaching are not observed.

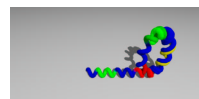
Bibliography

- [1] GA Blab, RA Bakker, R Leurs, and T Schmidt. Single molecule studies of the β_2 adrenergic receptor reveal aggregation before stimulation. -, in preparation, 2003.
- [2] HA Rockman, WJ Koch, and RJ Lefkowitz. Seven-transmembrane-spanning receptors and heart function. *Nature*, 415(6868):206–212, 2002.
- [3] SR George, BF O’Dowd, and SP Lee. G-protein-coupled receptor oligomerization and its potential for drug discovery. *Nature Reviews*, 1:808–820, October 2002.
- [4] RA Dixon, BK Kobilka, DJ Strader, JL Benovic, HG Dohlman, T Frielle, MA Bolanowski, CD Bennett, E Rands, and RE Diehl. Cloning of the gene and cDNA for mammalian beta-adrenergic receptor and homology with rhodopsin. *Nature*, 321(6065):75–79, 1986.
- [5] RJ Lefkowitz. The superfamily of heptahelical receptors. *Nature Cell Biology*, 2(7):E133–E136, 2000.
- [6] LF Agnati, S Ferre, C Lluís, R Franco, and K Fuxe. Molecular mechanisms and therapeutical implications of intramembrane receptor/receptor interactions among heptahelical receptors with examples from the striatopallidal GABA neurons. *Pharmacology Reviews*, 55(3): 509–550, 2003.
- [7] G Milligan. Oligomerisation of G-protein-coupled receptors. *Journal of Cell Science*, 114(Pt 7):1265–1271, 2001.
- [8] CD Rios, BA Jordan, I Gomes, and LA Devi. G-protein-coupled receptor dimerization: modulation of receptor function. *Pharmacol. Ther.*, 92(2-3):71–87, 2001.
- [9] S Angers, A Salahpour, and M Bouvier. Biochemical and biophysical demonstration of GPCR oligomerization in mammalian cells. *Life Sciences*, 68(19-20):2243–2250, 2001.
- [10] TE Hebert, S Moffett, JP Morello, TP Loisel, DG Bichet, C Barret, and M Bouvier. A peptide derived from a beta2-adrenergic receptor



- transmembrane domain inhibits both receptor dimerization and activation. *Journal of Biological Chemistry*, 271(27):16384–16392, 1996.
- [11] A Salahpour, H Bonin, S Bhalla, U Petaja-Repo, and M Bouvier. Biochemical characterization of beta2-adrenergic receptor dimers and oligomers. *Biol. Chem.*, 384(1):117–123, 2003.
- [12] TE Hebert, TP Loisel, L Adam, N Ethier, SS Onge, and M Bouvier. Functional rescue of a constitutively desensitized beta2ar through receptor dimerization. *Biochemical Journal*, 330 (Pt 1):287–293, 1998.
- [13] PR Gouldson, CR Snell, RP Bywater, C Higgs, and CA Reynolds. Domain swapping in G-protein coupled receptor dimers. *Protein Eng*, 11(12):1181–1193, 1998.
- [14] S Angers, A Salahpour, E Joly, S Hilaiet, D Chelsky, M Dennis, and M Bouvier. Detection of β_2 -adrenergic receptor dimerization in living cells using bioluminescence resonance energy transfer (BRET). *PNAS (USA)*, 97(7):3684–3689, 2000.
- [15] MC Dinger, JE Bader, AD Kobor, AK Kretzschmar, and AG Beck-Sickinger. Homodimerization of neuropeptide y receptors investigated by fluorescence resonance energy transfer in living cells. *Journal of Biological Chemistry*, 278(12):10562–10571, 2003.
- [16] R Latif, P Graves, and TF Davies. Ligand-dependent inhibition of oligomerization at the human thyrotropin receptor. *Journal of Biological Chemistry*, 277(47):45059–45067, 2002.
- [17] MC Overton and KJ Blumer. G-protein-coupled receptors function as oligomers in vivo. *Current Biology*, 10(6):341–344, 2000.
- [18] GJ Babcock, M Farzan, and J Sodroski. Ligand-independent dimerization of CXCR4, a principal HIV-1 coreceptor. *Journal of Biological Chemistry*, 278(5):3378–3385, 2003.
- [19] JF Mercier, A Salahpour, S Angers, A Breit, and M Bouvier. Quantitative assessment of beta 1- and beta 2-adrenergic receptor homo- and heterodimerization by bioluminescence resonance energy transfer. *Journal of Biological Chemistry*, 277(47):44925–44931, 2002.

- [20] D Ramsay, E Kellett, M McVey, S Rees, and G Milligan. Homo- and hetero-oligomeric interactions between G-protein-coupled receptors in living cells monitored by two variants of bioluminescence resonance energy transfer (BRET): hetero-oligomers between receptor subtypes form more efficiently than between less closely related sequences. *Biochemical Journal*, 365(Pt 2):429–440, 2002.
- [21] GS Harms, M Sonnleitner, GJ Schütz, HJ Gruber, and T Schmidt. Single-molecule anisotropy imaging. *Biophysical Journal*, 77:2864–2870, 1999.
- [22] T Schmidt, GJ Schütz, W Baumgartner, HJ Gruber, and H Schindler. Characterization of photophysics and mobility of single molecules in a fluid lipid membrane. *Journal of Physical Chemistry*, 99:17662–17668, 1995.
- [23] GS Harms, L Cognet, PHM Lommerse, GA Blab, H Kahr, HP Spaink, C Romanin, and T Schmidt. Imaging of L-type Ca^{2+} channels in live cells. *Biophysical Journal*, 81:2639–2646, 2001.
- [24] GS Harms, L Cognet, PHM Lommerse, GA Blab, and T Schmidt. Autofluorescent proteins in single-molecule research: Applications to live cell imaging microscopy. *Biophysical Journal*, 80:2396–2408, 2001.
- [25] PHM Lommerse, GA Blab, L Cognet, GS Harms, BE Snaar-Jagalska, HP Spaink, and T Schmidt. Single-molecule imaging of the h-ras membrane-anchor reveals domains in the cytoplasmic leaflet of the cell membrane. *Biophysical Journal*, in print, 2003.
- [26] EJG Peterman, S Brasselet, and WE Moerner. The fluorescence dynamics of single molecules of green fluorescent protein. *Journal of Physical Chemistry A*, 103:10553–10560, 1999.
- [27] P Schwille, S Kummer, AA Heikal, WE Moerner, and WW Webb. Fluorescence correlation spectroscopy reveals fast optical excitation-driven intramolecular dynamics of yellow fluorescent proteins. *PNAS (USA)*, 97(1):151–156, 2000.



This page intentionally contains only this sentence.

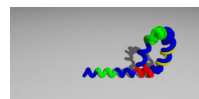
Chapter 4

Novel Single Nucleotide Pairing Assay using RCA

The work described in this chapter is published as “Homogenous detection of single rolling-circle replication products” in *Analytical Chemistry*.^[1]

4.1 Abstract

We describe a simple and straightforward approach for homogenous and isothermal detection of individual rolling-circle replication (RCR) products, which represent individual padlock probe circularization events. The RCR products consist of tens of kilobases long, single-stranded tandem repeated copies of the probe sequence, and in solution they fold into micron-sized random coils. The method is based on the local enrichment of fluorescence labeled probes that hybridize to the coiled RCR products compared to the



concentration of free probes in solution. We present a detailed characterization of the fluorescence labeled products using a highly sensitive and fast microscopy set-up. At a 10^4 -fold excess of free label we were able to detect and follow individual RCR products at a signal-to-background-noise ratio of 27. This high signal to background ratio leaves room for analysis in a simple detection device, at higher speeds or at lower labeling ratios.

4.2 Introduction

Probe circularization reactions with padlock probes allow sensitive and specific detection of DNA and RNA sequence variants[2–6]. In these studies padlock probes have been visualized in situ with fluorescence labeled antibodies or they have been amplified with PCR for subsequent analysis of the amplification product on gels or DNA micro-arrays. Rolling circle replication (RCR) specifically amplifies circularized probes, but the method suffers from limited sensitivity due to the linear mode of amplification[7, 8]. RCR generates a product that is different from most DNA molecules present in a typical biological sample, since the RCR product is a single-stranded tandem repeated copy of the circularized probe, typically thousand units long, and readily available for hybridization. Analysis of individual RCR products, representing single molecule detection events, has been described for analysis of RCR products in a solid phase based assay[9]. The detection efficiency was limited, however, probably due to slow hybridization kinetics on the flat glass surface used in the study.

In this paper we present a method for homogeneous and highly sensitive detection of RCR products in the presence of a ten thousand-fold excess

of unbound probes. The detection is performed in a microscope equipped with a flow system. The properties of labeled RCR products in solution are characterized, as well as the signal-contrast obtained between unbound fluorescence labeled probes and the ones bound to the RCR products. The figure-of-merit and the limitations of the novel method are discussed.

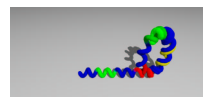
4.3 Experimental section

4.3.1 RCR template and probes

The RCR products were produced according to Nilsson et al. [8] using 180 fmol of the padlock probe pp93 (P-CCTCCCATCATATTAAGGCTT-TCTCTATGTTAAGTGACCTACG ACCTCAATGCTGCTGCTG-TACTACTCTTCCTAAGGCATTCTGCAAACAT, P = 5' phosphate), circularized on 540 fmol of the ligation target GCCTTTAATATGATGGGAGGATGTTTGCAGAATGCCTTAG, as polymerization substrate in a 90 μ l reaction volume. The Φ 29 DNA polymerase-catalyzed polymerization reaction (90 min, 37°C) was terminated by 5 min incubation at 65°C. The RCR products were diluted to 1 pM concentration in PBS and labeled using different combinations of 10 nM 5' rhodamine- or Cy5- labeled oligonucleotide RC1 (CTCTATGTTAAGTGACCTACG), and/or 5' rhodamine labeled oligonucleotide RC2 (GCTGCTGTACTACTCTTCCT).

4.3.2 High sensitivity detection

To detect the amplified rolling circle products, we utilized a high sensitivity imaging setup, described in detail previously[10–12]. A 10 μ m thick



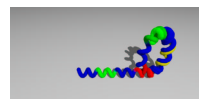
quartz precision cell (QS136, Hellma Benelux, Rijswijk, The Netherlands) was mounted onto a clean glass slide and subsequently fixed onto the microscope translation stage. The quartz cell allowed us to adjust a controlled flow through the detection volume and, in addition, confined the sample volume. Before adding the sample, the glass was coated with herring-sperm DNA to minimize unspecific binding of RCR products to the surface. While unspecific binding of the RCR products was effectively avoided in this way, a time-independent inhomogeneous background due to binding of detection oligonucleotides to herring-sperm DNA was observed. Because this background was static it was subtracted from the images, making identification of RCR-products straightforward (figures 4.4 and 4.5).

The microscope (Axiovert 100TV; Zeiss, Oberkochen, Germany) was equipped with a 10 \times Plan-Neofluar objective (NA = 0.3, Zeiss, Oberkochen, Germany). Samples were illuminated for 5 ms by the 532 nm line from a frequency-doubled Nd:YAG laser (Millenia X, Spectra Physics, Mountain View, CA, USA) for one color experiments. For two color experiments, the 514 nm line from an Argon-ion laser and 635 nm light from a tunable dye laser (model 3758, Spectra Physics, Mountain View, CA, USA) were used. The lasers were fiber-coupled into the microscope. A lens ($f = 5$ cm) focused the beam into the back focal plane of the objective leading to a lateral excitation profile of Gaussian shape with a width of $w = 120$ μm (full width at half-maximum). The mean illumination intensity, as calculated for the circular area of diameter w , was set to 0.2 kW/cm². The illumination was accurately timed via a combination of mechanical shutter (Uniblitz, Rochester, NY, USA) and acousto-optic modulator (AOM, Isomet, Springfield, VA, USA).

The use of appropriate filter combinations (one color experiments: dichroic 550DCLP and detection HQ 600/75, both Chroma Technology, Brattleboro, USA, in combination with OG570-3, Schott, Mainz, Germany; two-color experiments: dichroic: TMR/Cy5 dual filter set, Chroma Technology and OG 570-3 Schott) permitted highly sensitive and specific detection of the fluorescence by a liquid-nitrogen-cooled slow-scan CCD camera system ($20 \times 20 \mu\text{m}^2$ pixel size, Princeton Instruments, Trenton, NY, USA). A wedge-mirror simultaneously imaged two colors onto the surface of one CCD camera chip. The total detection efficiency of the experimental setup was about 1%. Images of 50×50 pixel ($100 \mu\text{m} \times 100 \mu\text{m} \times 7 \mu\text{m}$ depth of field) were taken every 100 ms, 500 images in sequence. An average background was computed from all images in a sequence and subtracted from each image before further analysis. To obtain accurate positional information and information on the signal level of the RCR products, we used a methodology developed in our lab for single-molecule tracking[13].

4.4 Results

The expected size estimated from the radius of gyration of a random coiled RCR product with 1000 copies of a 93 nt repeat is $2 \cdot \sqrt{1000/6} \cdot 30 \text{ nm} = 775 \text{ nm}$, which is smaller than the pixel size of $2 \mu\text{m}$. Hence, the signal expected from an RCR product that has bound 1000 fluorophores (one/repeat), is located in one pixel of the CCD chip. In comparison, at a concentration of 10 nM of unbound detection oligonucleotide, 170 fluorophores are located within the detection volume of one pixel of a CCD chip (voxel) of $2 \times 2 \times 7 \mu\text{m}^3$. Hence the RCR products are predicted to be



detectable at very high S/N ratio.

To test this prediction, padlock probes were circularized using an excess of target oligonucleotide ligation templates. The ligation templates further acted as primers in the subsequent 90 min RCR, which generates products containing 1000-1500 copies of the probe sequence[7]. The RCR products were diluted to 1 pM and subsequently incubated with 10 nM of fluorescence labeled detection oligonucleotides, complementary to a sequence present in each repeat of the tandem repeated single-stranded RCR products. Lower concentrations of detection oligonucleotide did not affect the background fluorescence significantly, and higher concentrations did not increase the signal significantly (not shown).

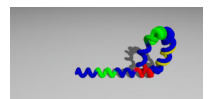
After subtraction of the static background signal (figure 4.5), individual RCR products appearing as signals with a lateral dimension $< 2 \mu\text{m}$, matching the point-spread function of the optical detection system, were clearly detectable even in the presence of a 10^4 -fold excess of free labeled oligonucleotides (figure 4.2A-C). The mean signal to background ratio seen in figure 4.2A-C amounts to $S/B = 1$ somewhat lower than the predicted value of 1000/170. However, relevant for identification is the mean signal to background-noise ratio, ($S/N = S/\sqrt{B} = 27$) which was much larger than unity, rendering single RCR product imaging straight-forward. Negative control experiments were performed by omitting the incubation step with ligase. In those experiments we were unable to find any signals beyond noise after subtraction of the constant background signal.

Since RCR products appeared as point-like objects analytical methods developed for single-molecule studies were employed for further characterization. Individual RCR products were followed as they moved along with

the flow of buffer through the detection volume (figure 4.2D). By their linear mobility they were clearly distinguishable from the inhomogeneous background. Further analysis of the trajectories revealed a flow speed of $\simeq 10 \mu\text{m/s}$, which translates to a screening volume of 0.5 nl/min. This speed of flow allowed accurate identification of the DNA particles in the solution with a camera readout speed of 10 images/s and illumination time of 5 ms. It should be noted, however, that the fairly low flow speed is not inherent to the method presented in this paper and can be increased to at least $100 \mu\text{m/s}$ without smearing of signals within the 5 ms illumination time.

The signal level of the RCR products was further analyzed to obtain information about labeling efficiency and possible aggregation (Fig. 4.3). As the Gaussian illumination profile had a FWHM larger than the imaged area, no correction for changes in intensity was performed. We obtained mean signal values of $637 \pm 64 \text{ cts}/5 \text{ ms}$ and $858 \pm 86 \text{ cts}/5 \text{ ms}$ for RCR products labeled with rhodamine and Cy5, respectively. As the Gaussian illumination profile had a width larger than the imaged area, a correction for variation in intensity with position was omitted (figure 4.4).

Taking into account the expected signal from an individual fluorophore^[10] of $1.8 \pm 0.2 \text{ cts}/5 \text{ ms}$ and $3.2 \pm 0.3 \text{ cts}/5 \text{ ms}$ for rhodamine and Cy5, respectively, at the present illumination intensity and detection efficiency, the RCR products generate signals that correspond to 300-350 pure fluorophores per RCR product. This number deviates substantially from the expected number of fluorophore-labeled oligonucleotides hybridizing to the 1000-1500 repetitions of the 93 nt motif. This discrepancy can be either due to incomplete hybridization, or more likely due to quenching caused



by electronic interactions between the fluorophores and the nucleobases, or with themselves at high packing. It has been shown from numerous studies that both rhodamine and Cy5 are sensitive to their local environment leading to self-quenching[14], base-specific quenching on binding to DNA[15] or even anomalous enhancement upon binding to proteins[16]. We have further shown that fluorescence from labeled oligonucleotides may be quenched by a factor of two when hybridized to intact RCR products, as compared to the same product in monomer form[8].

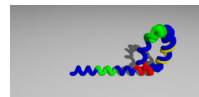
The intensity distributions for both detection oligonucleotides show features consistent with aggregation of two RCR products (figure 4.3). For the rhodamine labeled products a clear shoulder at 1301 cnts/5 ms is visible in the signal distribution (figure 4.3 left). The intensity distributions were further analyzed for two populations of single and double product formation utilizing a strategy developed earlier in our laboratory[17]. This method allows us to attribute an average stoichiometry to a whole population of products, even when the assignment may be difficult due to the large spread in intensities. Applying this strategy we found that $47 \pm 5\%$ of the RCR products occurred as single products and $53 \pm 5\%$ as double products for the rhodamine labeled products, and $63 \pm 6\%$ “singels” and $37 \pm 4\%$ “doubles” for the Cy5-labeled products. No separation-events of such “double” complexes were observed, leading to the conclusion that the complexes were stable over minutes. We have further noticed that aggregation of RCR products is promoted by high concentrations of BSA present in the polymerization buffer and can be avoided by modifying the buffer composition (J. Jarvius, personal communication).

4.5 Discussion

We have demonstrated the applicability of a homogeneous flow assay for the detection and analysis of 90 kb RCR products. Both rhodamine and Cy5-labeled RCR products show strong localized fluorescence, which was detected against the background of 10 nM labeled detection oligonucleotides, a concentration that seems sufficient to saturate the RCR products with labels.

Further, different fluorescence labels can be studied simultaneously, opening the possibility of parallel detection of several DNA sequences, or the further enhancement of detection sensitivity by coincidence analysis. In preliminary experiments we have applied a dual-color detection scheme[11] for detection of RCR products (figure 4.6). RCR products were labeled with both rhodamine and Cy5 labeled oligonucleotides at equimolar concentration. Clearly particles were identified in both channels with some of the particles showing fluorescence resonance energy transfer which would increase the specificity of this assay even further.

In general, analysis of individual single DNA sequences in complex DNA samples has been realized so far by detecting the coincident binding of two oligonucleotides labeled with two different fluorophores[18–20]. The present approach avoids problems of nonspecific background since detection events require coincident binding of many oligonucleotides to individual RCR products. Furthermore, the signal generated from hundreds of fluorophores allows faster detection with less advanced detection devices, compared to the set-up required for single fluorophore detection. With appropriate means of controlling the flow, as realized by microfluidics, the



screening of larger amounts (microliters) of solution within minutes will be possible, making our approach a viable means of biological and medical testing.

We expect that the method will present great advantages for multiplexed measurements of gene expression levels. Since differentially labeled RCR products are spatially resolved, a minority product will be detectable also in a large excess of other products, resulting in a high dynamic analysis range. Moreover, the quantitative precision should be superior to bulk measurements, since the precision of the present digital approach should ultimately be limited only by the statistical sampling error. We currently apply this methodology in a microfluidic set-up which can be mounted in either a conventional or a confocal fluorescence microscope (Jarvius et al., in preparation).

4.6 Acknowledgement

Dr. Ulf Landegren and Dr. Anton K. Raap contributed valuable comments. This work was supported by a long term EMBO fellowship to MN and a joint travel grant from the Dutch and Swedish research councils. MN is further supported by grants from the Bergström Foundation, Svenska Läkaresällskapet, and the Swedish research council for Medicine. We thank Carl Zeiss for the loan of the 10× objective.

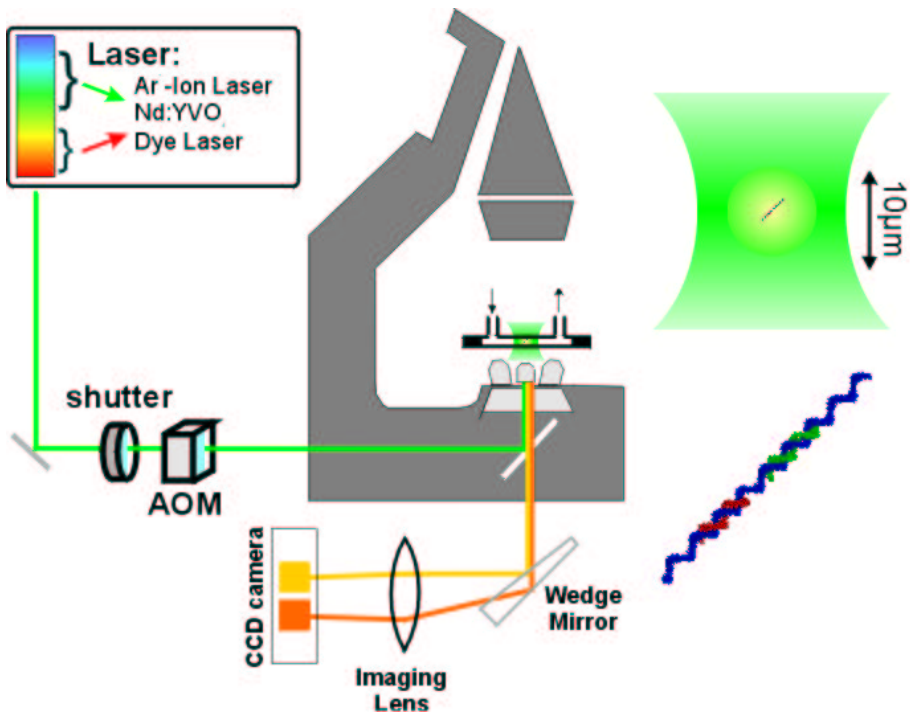
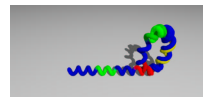


Figure 4.1: Schematic representation of the setup. A shutter and an acousto-optic modulator (AOM) control the timing of the laser illumination; the 10 μm high cuvette is homogeneously illuminated and the emitted fluorescence is collected; a wedge mirror allows to split the image into a yellow (Rhodamine, top) and red (Cy5, bottom) channel, both of which can be imaged simultaneously. The cartoon on the left shows one 93 nt repeat of the DNA (blue) and the positions of the two probes (green and red, respectively). The DNA is not drawn to scale.



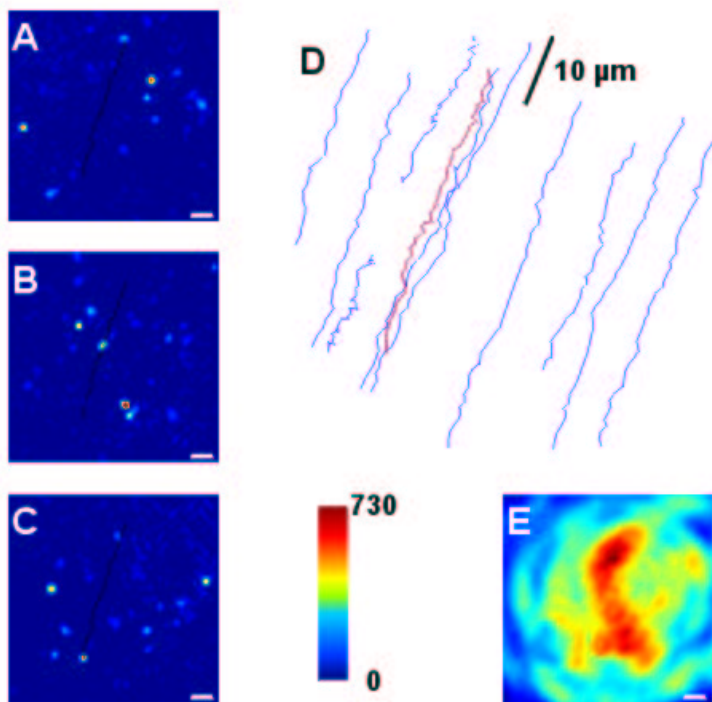


Figure 4.2: (A-C) Three images in a series of 54 images following a particular piece of DNA. The full trace is shown in black in all images. (D) Traces from 11 different pieces of DNA which could be followed for more than 30 images in one sequence (500 images); the trace from (A-C) is shown in red. The flow as calculated from the end-to-end distances of the traces is approximately $10\mu\text{m/s}$. (E) Mean background of the sequence, which has been subtracted before further processing. The scale bar in all images is $10\mu\text{m}$.

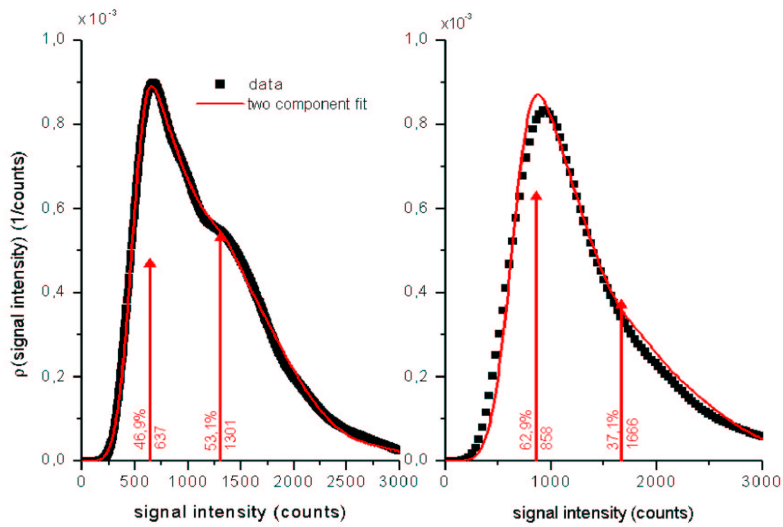
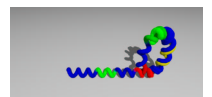


Figure 4.3: Distribution of fitted intensities for Rhodamine (left) and Cy5-labelled DNA. A fit of both distributions indicates that 40-50% of the particles observed are actually two strands of DNA.



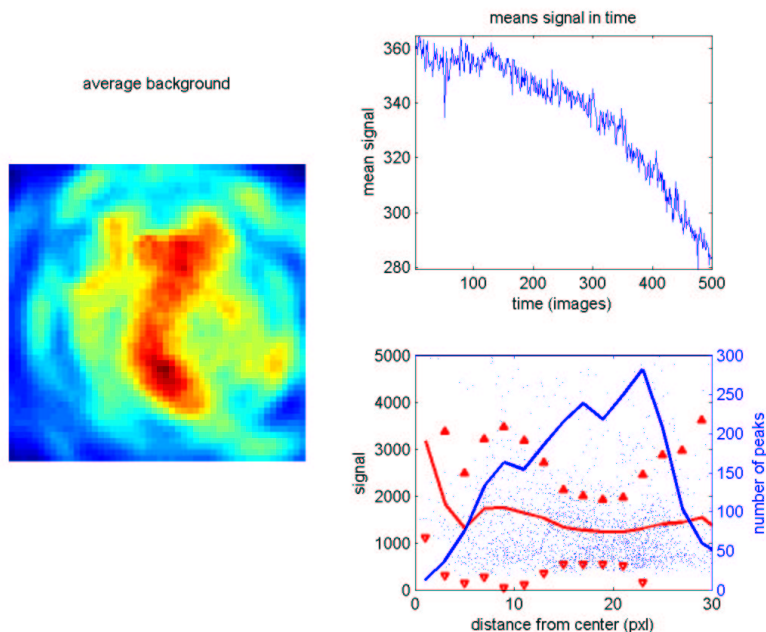


Figure 4.4: The fluorescent features caused by unspecific binding of oligonucleotide-probes to the herring-sperm coated surface stay constant in time (left). The mean background signal bleaches slowly over the course of 500 images (right top).

The analysis of intensities from individual RCR products (bottom right, dots) shows no strong correlation with the distance from the center of the laser profile (line: sliding average, triangles: standard deviation). The number of RCR products found at different distances from the center is given by the dark line.

The size of the image is $100 \mu\text{m}$; the laser profile is $120 \mu\text{m}$ wide. Time per image is 5 ms.

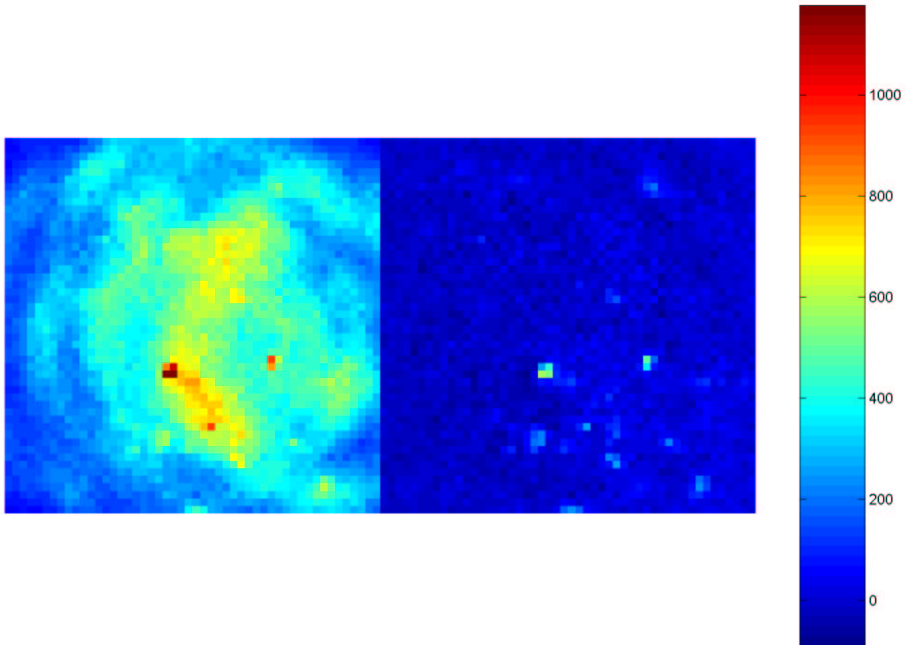
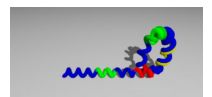


Figure 4.5: The background subtraction uses the fact that the fluorescent features of the background are constant in time. The image and the movie show the raw data used to generate the traces in figure 4.2 (left), and the same image after background subtraction (right).

The size of each image is $100 \mu\text{m}$.



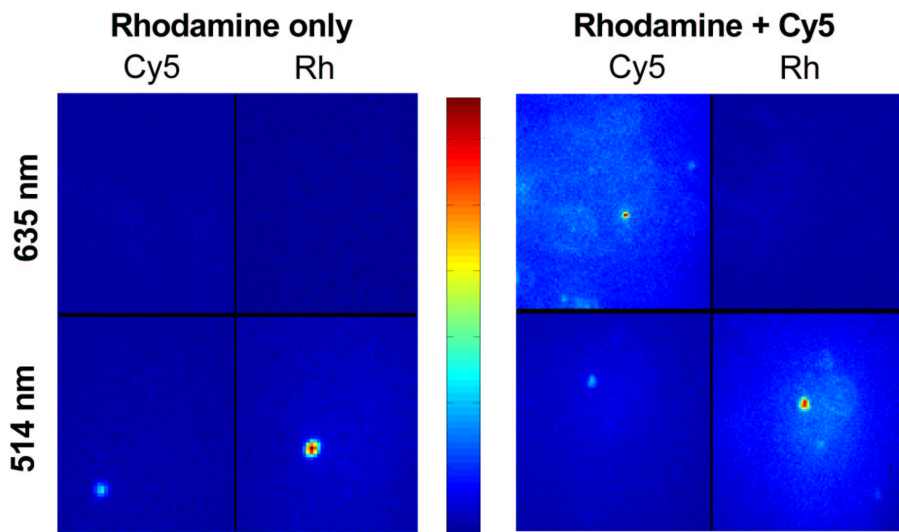
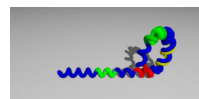


Figure 4.6: Comparison between RCR products labeled only with Rhodamine (left) and those labeled with Rhodamine and Cy5 (right). The excitation alternated between 635nm (Cy5 excitation; top) and 514nm (Rhodamine excitation; bottom). A 25% “bleed-through” of Rhodamines signal into the Cy5-channel is observed (bottom left and right). The signal from Cy5 was collected in the left channels, the signal from Rhodamine in the right channels. The images have been corrected for a slight vertical offset caused by the alignment of the wedge mirror.

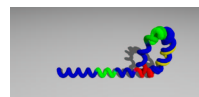
Bibliography

- [1] GA Blab, T Schmidt, and M Nilsson. Homogeneous detection of single RCR products. *Analytical Chemistry*, in press, 2003.
- [2] M Nilsson, H Malmgren, M Samiotaki, M Kwiatkowski, BP Chowdhary, and Landgren U. Padlock probes: Circularizing oligonucleotides for localized DNA detection. *Science*, 265:2085–2088, 1994.
- [3] M Nilsson, K Krejci, J Koch, M Kwiatkowski, P Gustavsson, and U Landgren. Padlock probes reveal single-nucleotide differences, parent of origin and in situ distribution of centromeric sequences in human chromosomes 13 and 21. *Nature Genetics*, 16:252–255, 1997.
- [4] M Nilsson, G Barbany, Antson D-O, K Gertow, and U Landegren. Enhanced detection and distinction of rna by enzymatic probe ligation. *Nature Biotechnology*, 18:791–793, 2000.
- [5] P Hardenbol, J Banér, M Jain, M Nilsson, EA Namsaraev, GA Karlin-Neuman, H Fakhrai-Rad, M Ronaghi, TD Willis, and U Landegren. Highly multiplexed genotyping with sequence-tagged molecular inversion probes and DNA microarrays. *Nature Biotechnology*, in press, 2003.
- [6] J Banér, A Isaksson, E Waldenström, J Jarvius, U Landegren, and M Nilsson. Parallel gene analysis with allele-specific padlock probes and tag microarrays. *Nucleic Acids Research*, 31(17):e103, 2003.
- [7] J Banér, M Nilsson, M Mendel-Hartvig, and U Landegren. Signal amplification of padlock probes by rolling circle replication. *Nucleic Acid Research*, 22:5073–5078, 1998.
- [8] M Nilsson, M Gullberg, F Dahl, K Szuhai, and AK Raap. Real-time monitoring of rolling-circle amplification using a modified molecular beacon design. *Nucleic Acids Research*, 30:e66, 2002.
- [9] PM Lizardi, X Huang, Z Zhu, P Bray-Ward, DC Thomas, and DC Ward. Mutation detection and single-molecule counting using isothermal rolling-circle amplification. *Nature Genetics*, 19(3):225–232, 1998.



- [10] T Schmidt, GJ Schütz, W Baumgartner, HJ Gruber, and H Schindler. Characterization of photophysics and mobility of single molecules in a fluid lipid membrane. *Journal of Physical Chemistry*, 99:17662–17668, 1995.
- [11] L Cognet, GS Harms, GA Blab, PHM Lommerse, and T Schmidt. Simultaneous dual-color and dual-polarization imaging of single molecules. *Applied Physics Letters*, 77:4052, 2000.
- [12] GS Harms, L Cognet, PHM Lommerse, GA Blab, and T Schmidt. Autofluorescent proteins in single-molecule research: Applications to live cell imaging microscopy. *Biophysical Journal*, 80:2396–2408, 2001.
- [13] GJ Schütz, H Schindler, and T Schmidt. Single-molecule microscopy on model membranes reveals anomalous diffusion. *Biophysical Journal*, 73:1073–1080, 1997.
- [14] RI MacDonald. Characteristics of self-quenching of the fluorescence of lipid- conjugated rhodamine in membranes. *Journal of Biological Chemistry*, 265(23):13533–13539, 1990.
- [15] CAM Seidel, A Schulz, and MHM Sauer. Nucleobase-specific quenching of fluorescent dyes. 1. nucleobase one-electron redox potentials and their correlation with static and dynamic quenching efficiencies. *Journal of Physical Chemistry*, 100:5541–5553, 1996.
- [16] HJ Gruber, CD Hahn, G Kada, CK Riener, GS Harms, W Ahrer, TG Dax, and HG Knauss. Anomalous fluorescence enhancement of Cy3 and Cy3.5 versus anomalous fluorescence loss of Cy5 and Cy7 upon covalent linking to IgG and noncovalent binding to avidin. *Bioconjugate Chemistry*, 11(5):696–704, 2000.
- [17] T Schmidt, GJ Schütz, W Baumgartner, HJ Gruber, and H Schindler. Imaging of single molecule diffusion. *PNAS (USA)*, 93:2926–2929, 1996.
- [18] A Castro and JGK Williams. Single-molecule detection of specific nucleic acid sequences in unamplified genomic DNA. *Anal. Chem.*, 69 (19):3915–3920, 1997.

- [19] A Castro and RT Okinaka. Ultrasensitive, direct detection of a specific DNA sequence of bacillus anthracis in solution. *Analyst*, 125(1):9–11, 2000.
- [20] MB Wabuye, H Farquar, W Stryjewski, RP Hammer, SA Soper, Y-W Cheng, and F Barany. Approaching real-time molecular diagnostics: Single-pair fluorescence resonance energy transfer (spFRET) detection for the analysis of low abundant point mutations in k-ras oncogenes. *J. Am. Chem. Soc.*, 125(23):6937–6945, 2003.



This page intentionally contains only this sentence.

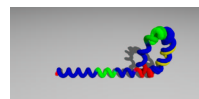
Chapter 5

Simultaneous Wide-Field Imaging and Spectroscopy of Localized Fluorophores

The work described in this chapter is published as “Simultaneous Wide-Field Imaging and Spectroscopy of Localized Fluorophores” in *Optical Letters*.^[1]

5.1 Abstract

A method that combines fluorescence imaging and spectroscopy of single molecules at room temperature is presented. This approach allows us to identify a number of imaged molecules unequivocally by simultaneously recording their fluorescence emission spectra. Furthermore, the spectral characteristics not only allow us to separate different fluorescent labels



quantitatively and qualitatively, but also provide information on the microenvironment of the molecules. This new method was successfully tested on a system of yellow-green and red fluorescent 20 nm latex beads and its benefit for the studies on biological systems was illustrated on a preparation of COBRA-stained mouse chromosomes.

5.2 Introduction

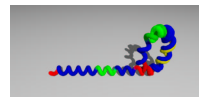
Advancements in optical methods and improvement of imaging equipment currently allow the routine application of ultra-sensitive fluorescence microscopy at the level of an individual molecule[2–4]. This development is particularly important in analytical chemistry and holds large promise for the biosciences. For the latter the detection and localization of molecular species present at very low concentration (a few copies per cell) is essential. Studies of molecular conformational dynamics, molecular interactions, and processes involved in signaling cascades are currently underway[5]. However, in multi-component systems like cells or biomolecular screening assays, one needs to go beyond mere detection and localization of one molecule to simultaneous, unequivocal identification of all components involved. The continued development of techniques to specifically label molecular species by selected fluorescence tags[4, 6, 7] allows the identification of a molecule by its fluorescence spectrum, which can also be used to obtain additional information about the local environment of the molecule. Hence, there is a general need for fast, parallel imaging technology with added spectral information. So far, technical solutions rely on confocal imaging[8], consecutive imaging with different emission filter sets[9], or on consecutive imaging with

different excitation wavelength[10, 11]. In a recent development, we have described a simple imaging scheme utilizing a dichroic wedge in the infinity path of a microscope to simultaneously acquire dual-color information on one CCD-camera[12].

A generalization of this scheme, which allows for simultaneous acquisition of image and spectrum, is presented here. In place of the dichroic wedge we mounted a blazed reflective grating into the infinity beampath of a microscope (figure 5.1). The dispersion of the grating was chosen such that both the zero'th and first order of diffraction were imaged onto the same CCD-camera. Thereby we obtained information on both the localization and the emission spectra of fluorescent objects which are sparsely distributed in the focal plane of the microscope. A similar approach has been described by Ma et al. [13], using a transmission grating which had the disadvantage that the intensity ratio between the zero'th and first order can not be adjusted. To test the applicability of our concept we used immobilized 20 nm fluorescent latex beads, and multiplex stained mouse chromosomes to demonstrate the biological applicability.

5.3 Experimental Setup

The experimental setup is based on the one described in detail previously[12]. In short, the samples were mounted onto an inverted microscope (Zeiss Axiovert100), imaged through a high aperture, 100 \times oil-immersion objective (Zeiss, NA=1.4), and illuminated for 10 to 50 ms with a single line from an Ar⁺-laser, or at 625 nm from a dye laser (both Spectra Physics). The excitation light was suppressed in the detection path by use of an appropriate fil-



ter combination (chromatic beam-splitter, bandpass 514/560DBM, Chroma Technology; Holographic Super-Notch 488-1.0, Kaiser Optics; long-pass OG and RG filters, Schott). The blazed reflection grating (60 grooves/mm, 1.26° nominal blaze angle; Thermo RGL) was placed in the infinity path of the microscope (figure 5.1). A 150 mm achromatic lens focused the zero'th and first order reflections onto a back-illuminated, liquid-nitrogen-cooled CCD camera (400 × 1340 pixels, 20 × 20 μm² pixel size, LN/CCD-400-PB, Princeton Instruments), forming an image and a first-order spectrum simultaneously.

5.4 Results and Discussion

5.4.1 Calibration

A spectral calibration was carried out with the lines of the Ar⁺-laser, and the dye laser. The spectral separation d between the zero'th order and the first order for wavelength, λ , is determined by the grating equation,

$$d = f \cdot \tan \left(\arcsin \left(-\frac{\lambda}{g} - \sin \theta \right) + \theta \right) \quad (5.1)$$

where the focal length of the imaging lens, f , the angle of the incoming light, $\theta \approx 45^\circ$, and the grating constant, g . Equation 5.1 can be approximated as a linear relationship over the wavelength range of interest (500-700 nm) due to a small angular separation of $< 4^\circ$. The separation is characterized by the lateral dispersion of $D = 1.5 \text{ nm/pxl}$. The blazing angle was chosen such that over the whole wavelength range of interest $> 65\%$ of the light was distributed to the first order. The total detection efficiency was better than 6% for all fluorophores used.

The almost linear dispersion makes a calculation of the spectral image in the first order simple. Given the intensity distribution of the zero'th order image, $I(x, y)$, being described by the sum of N separated molecular species $I(x, y) = \sum_i f_i(x, y)$, and the spectrum of each molecular species $s_i(\lambda)$, the first-order spectral image, $S(x, y)$, is given by the convolution,

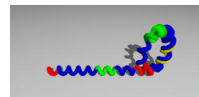
$$S(x, y) = \sum_i^N \int d\lambda f_i(x, y) \cdot s_i(\lambda) \quad (5.2)$$

There are two cases where analysis is most straightforward: (i) imaging of a single species ($N = 1$) of unknown spectrum for which $s(\lambda)$ can be determined by image deconvolution, and (ii) imaging of multiple species of known spectra for which equation 5.2 can be used to identify signals in $I(x, y)$ to originate from a certain species. Both approaches have been employed in our initial experiments.

5.4.2 Nanometer-sized fluorescent beads

First, we tested our methodology on fluorescently labeled yellow-green and red 20 nm latex beads (Molecular Probes). Samples of both beads were spin-coated on HF-etched microscope cover slips to a surface concentration of $< 0.1 \mu\text{m}^{-2}$ and were excited at 488 nm with $0.5 \text{ kW}/\text{cm}^2$ and 514 nm with $2 \text{ kW}/\text{cm}^2$, for the yellow-green and red beads, respectively. Individual beads were detected at a signal-to-noise ratio of typically $S/N = 30$ in the zero'th-order image and the corresponding spectrum to each bead was identified in first-order (figure 5.2B).

Given the background noise of our camera system of $b = 6 \text{ cnts}/\text{pxl}$ (limited by the read-out noise), the width of a spectrum, w , of approximately



40 pixel (equivalent to ≈ 60 nm), and a total signal of $S = 9000$ counts collected for an individual bead, the signal-to-background noise ratio in a worst-case broad spectrum without features equals to $S/B = S/(2 \cdot b \cdot w) = 19$. In reality, however, the peak of a fluorescence distribution can exhibit an S/B ratio of up to one order of magnitude higher. At this high S/B ratio, deconvolution of the spectral image is straightforward. In the case of wavelength-delimited objects such as those shown in figure 5.2, the deconvolution step can be omitted completely. In either case this leads to the spectrum of the fluorescent beads given in figure 5.2B for the yellow-green and red species, respectively. The resulting spectra show an excellent agreement with the corresponding bulk fluorescence emission spectra. This demonstrates the suitability of the new technique for obtaining fluorescence emission spectra of individual particles with very good spectral resolution and quality.

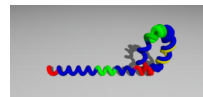
Each bead contains about 180 fluorophores (Molecular probes product sheet). Taking this and the above estimated S/B ratio into account, we extrapolate that we can obtain a quantifiable spectrum from the signal of just 10 molecules without further experimental refinement at an illumination time of just 50 ms.

5.4.3 COBRA-FISH-stained mouse chromosomes

We also tested whether our methodology was able to localize and identify a species in a mixture of different fluorescent species. This is a typical problem encountered in chromosomal assays or karyotyping in which either colors are used to code for a specific chromosome (multicolor in situ hybridization (MFISH)[14, 15]), or in which a unique mixture of col-

ors is used to code for the different chromosomes (combined binary ratio labeling in situ hybridization (COBRA-FISH)[16]). Here we studied COBRA-stained mouse chromosomes, carrying four different fluorescent labels (DEAC, FTIC, Cy3, and Cy5). Mouse fibroblast were arrested in metaphase by treatment with colcemide, swelled in hypotonic KCl solution, and fixed with methanol/acetic acid (3+1 v/v). This preparation was then dropped onto clean microscope slides, which resulted in random spreading of the chromosomes[17, 18] over an area of several μm^2 (figure 5.3A).

In our experiment we concentrated on three of the dyes (FITC, Cy3, Cy5), by simultaneously exciting the sample at 514 and 625 nm. Figure 5.3 shows an image containing 9 separable chromosomes (figure 5.3A) and their spectra (figure 5.3B). In order to analyze the overlapping spectra in this experiment we utilized a non-linear fitting procedure to find the labeling ratios in each of the $N = 3$ dyes accessible for every chromosome. For this, chromosome locations were first identified by thresholding. Subsequently, equation 5.2 in combination with the normalized bulk spectra, s_i of FITC, Cy3, and Cy5 respectively, was used to generate a spectral image with the intensity values ($I_{FITC}, I_{Cy3}, I_{Cy5}$) as free parameter for each chromosome (figure 5.3D). Fitting yielded the respective intensity values for each chromosome. The resulting chromosome identification image is shown in figure 5.3C. Not all chromosomes could be assigned uniquely, as we lacked information on the fourth label (DEAC) in the near UV. While the non-linear fitting procedure works well for sparsely distributed species even in the case of overlapping spectral images (as shown in figure 5.3), this procedure will be increasingly error-prone for higher density samples. In this case, fluorescence labels with sharper spectra[19], leading to less overlap



in the spectral image, will be of advantage. Additional optimization and testing will be needed to assess whether our methodology will be applicable to high-density samples like DNA-chips.

5.5 Conclusions

In conclusion, we have presented a new method to simultaneously record fluorescence images and fluorescence emission spectra at high quality and spectral resolution, with an estimated sensitivity of about 10 single fluorophores. This new simple, robust, yet highly sensitive method can easily be incorporated in existing imaging setups. The speed of acquisition is limited only by the amount of signal that can be obtained from the sample and ranges from several images per second to video-rate and above. In turn, this lower time limit sets an upper limit to the speed of moving object which can be analyzed before smearing-out will occur in the image (at video-rate $\approx 7\mu\text{m/s}$). Indeed, any number of different fluorophores can be imaged simultaneously, provided that the emitting species are sparsely distributed over the field-of-view. We have shown that this methodology is suited for a variety of applications in life-science research.

5.6 Acknowledgments

Hans Tanke and Joop Wigand for providing us with a COBRA stained chromosomes. S. Oellerich acknowledges financial support from the European Marie Curie Fellowship program. Gregory Harms and Laurent Cognet are acknowledged for their valuable input at the early stages of this project.

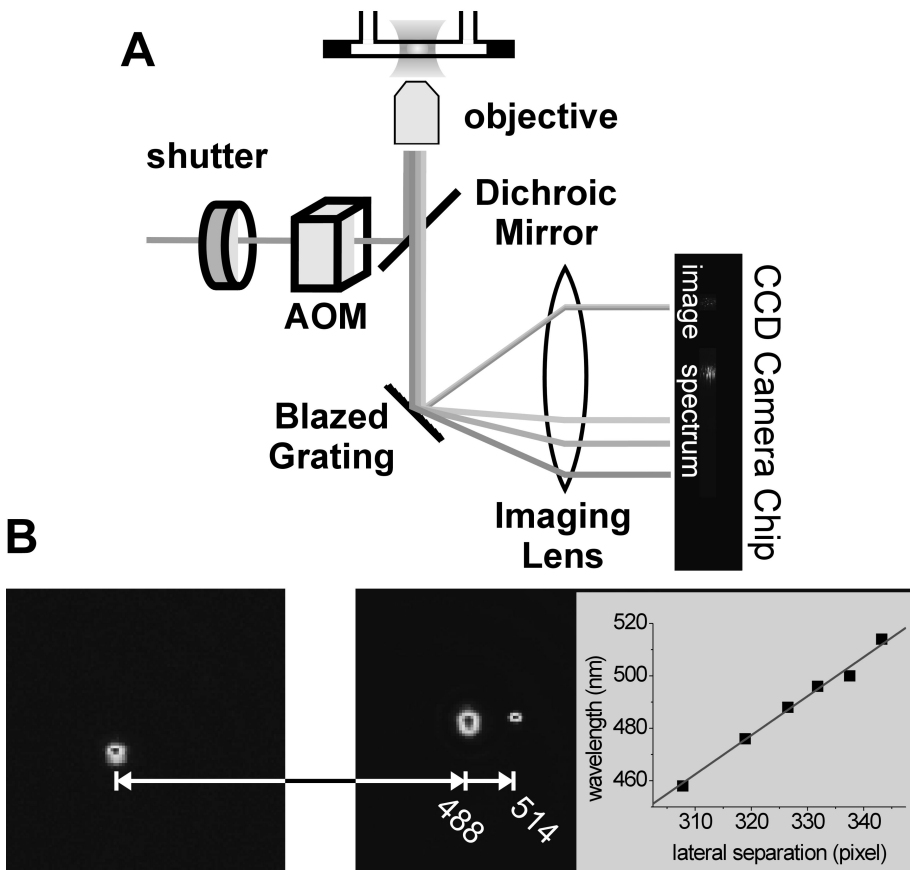
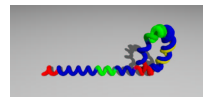


Figure 5.1: **(A)** Experimental setup. The fluorescence image and spectrum of the sample are simultaneously formed on the CCD camera as the zero'th and first order diffraction from a blazed grating placed in the infinity beam path of the microscope and subsequently focused onto the chip. **(B)** Zoom into A; a wavelength calibration of the dispersed image is shown by the refraction of two out of six lines from an Ar⁺ laser; the inset on the right shows all six measured positions, resulting in a first order calibration.



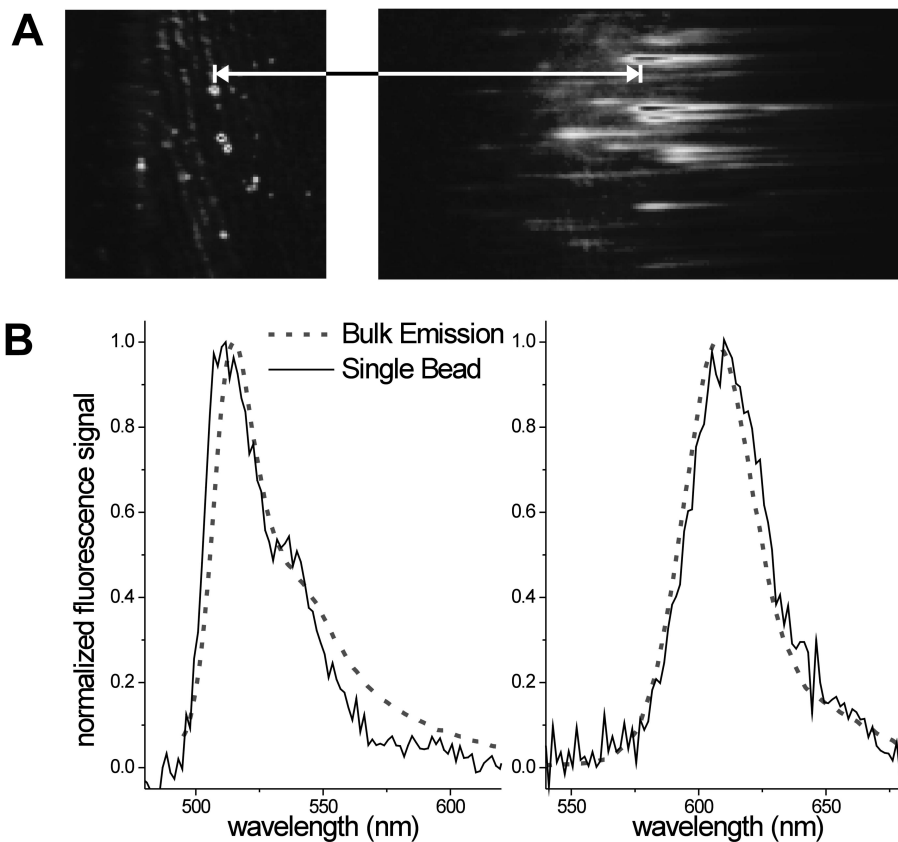


Figure 5.2: **(A)** Image and Spectrum of yellow 20 nm beads. Starting from one bead one can accurately determine the distance between zero'th and first order, which are slightly offset in this example. The distance between zero'th and first order (arrow) can be used to determine a wavelength scale using the calibration shown in figure 5.1B. **(B)** Spectra obtained from individual yellow-green (left) and red (right) 20 nm beads (solid lines) in comparison with the corresponding bulk spectra (dotted lines).

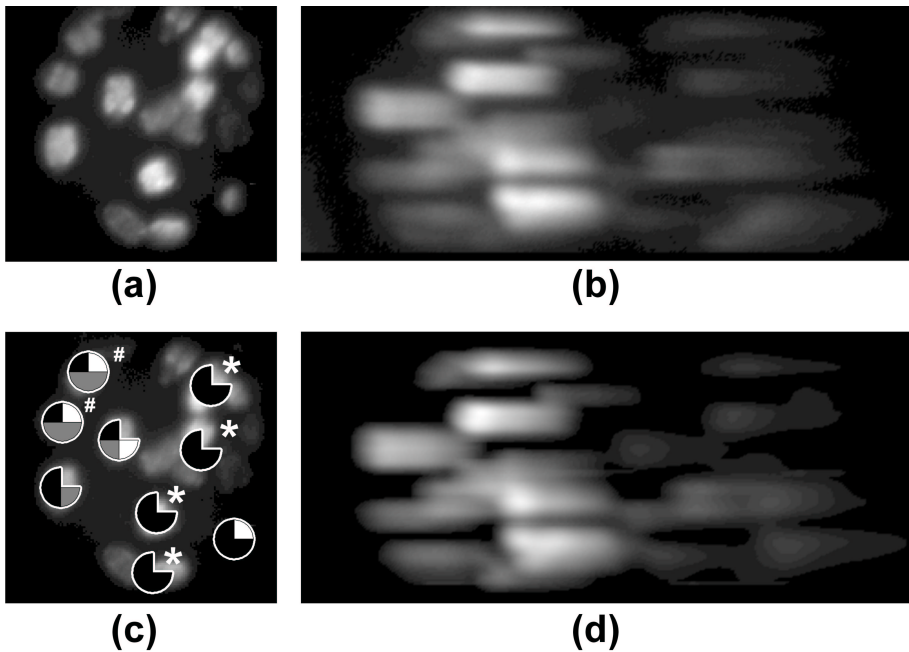
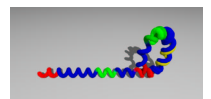


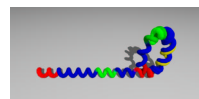
Figure 5.3: Simultaneous illumination at 514 nm and 625 nm of metaphasic mouse chromosomes with COBRA-FISH staining. Several chromosomes can be identified in the zero'th (**A**, $30 \times 30 \mu\text{m}^2$) and first order image (**B**). A least-square fit according to equation 5.2 (typical result in **D**) allows us to assign labeling ratios of the three different fluorophores to each chromosome (pie-charts in **C**). As the full labeling consists of four distinct colors, the chromosomes marked * and # can not be uniquely identified.



Bibliography

- [1] GA Blab, S Oellerich, R Schumm, and T Schmidt. Simultaneous wide-field imaging and spectroscopy of localized fluorophores. *Optics Letters*, in press, 2003.
- [2] GJ Schütz, H Schindler, and T Schmidt. Single-molecule microscopy on model membranes reveals anomalous diffusion. *Biophysical Journal*, 73:1073–1080, 1997.
- [3] WE Moerner and M Orrit. Illuminating single molecules in condensed matter. *Science*, 283:1670–1676, 1999.
- [4] GS Harms, L Cognet, PHM Lommerse, GA Blab, and T Schmidt. Autofluorescent proteins in single-molecule research: Applications to live cell imaging microscopy. *Biophysical Journal*, 80:2396–2408, 2001.
- [5] T Ha, X Zhuang, HD Kim, JW Orr, JR Williamson, and S Chu. Ligand-induced conformational changes observed in single rna molecules. *PNAS (USA)*, 96(16):9077–9082, 1999.
- [6] VW Cornish, DR Benson, CA Altenbach, K Hidek, WL Hubbell, and PG Schultz. Site-specific incorporation of biophysical probes into proteins. *PNAS (USA)*, 91:2910–2914, 1994.
- [7] S Weiss. Fluorescence spectroscopy of single biomolecules. *Science*, 283:1676–1683, 1999.
- [8] A van Oijen, M Ketelaars, J Köhler, TJ Aartsma, and J Schmidt. Unraveling the electronic structure of individual photosynthetic pigment-protein complexes. *Science*, 285:400–402, 1999.
- [9] GJ Schütz, W Trabesinger, and T Schmidt. Direct observation of ligand colocalization on individual receptor molecules. *Biophysical Journal*, 74:2223–2226, 1998.
- [10] T Schmidt, GJ Schütz, W Baumgartner, HJ Gruber, and H Schindler. Imaging of single molecule diffusion. *PNAS (USA)*, 93:2926–2929, 1996.
- [11] JM Caruge and M Orrit. Investigations of local currents in a semicon-

- ductor by single-molecule spectroscopy. *Journal of Luminescence*, 98: 1–5, 2002.
- [12] L Cognet, GS Harms, GA Blab, PHM Lommerse, and T Schmidt. Simultaneous dual-color and dual-polarization imaging of single molecules. *Applied Physics Letters*, 77:4052, 2000.
- [13] Y Ma, MR Shortreed, and ES Yeung. High-throughput single-molecule spectroscopy in free solution. *Analytical Chemistry*, 72:4640–4645, 2000.
- [14] MR Speicher, BS Gwyn, and DC Ward. Karyotyping human chromosomes by combinatorial multi-fluor FISH. *Nature Genetics*, 12: 368–375, 1996.
- [15] E Schröck, S du Manoir, T Veldman, B Schoell, J Wienberg, MA Ferguson-Smith, W Ning, DH Ledbetter, I Bar-Am, D Soenksen, Y Garini, and T Ried. Multicolor spectral karyotyping of human chromosomes. *Science*, 273:494–497, 1996.
- [16] HJ Tanke, J Wiegand, RPM van Gijlswijk, V Bezrookove, H Pattenier, RJ Heetebrij, EG Talman, AK Raap, and J Vrolijk. New strategy for multi-colour fluorescence in situ hybridisation: COBRA: COmbined Binary RAtio labeling. *European Journal of Human Genetics*, 7:2–11, 1999.
- [17] J Wiegant, T Ried, PM Nederlof, P M van der Ploeg, HJ Tanke, and AK Raap. In situ hybridization with fluoresceinated DNA. *Nucleic Acid Research*, 1991.
- [18] J Wiegant, CC Wiesmeijer, JM Hoovers, E Schuurin, A d’Azzo, J Vrolijk, HJ Tanke, and AK Raap. Multiple and sensitive fluorescence in situ hybridization with rhodamine-, fluorescein-, and coumarin-labeled dnas. *Cytogenet Cell Genet*, 63:73–76, 1993.
- [19] TD Lacoste, X Michalet, F Pinaud, DS Chemla, AP Alivisatos, and S Weiss. Ultrahigh-resolution multicolor colocalization of single fluorescent probes. *PNAS (USA)*, 97(17):9461–9466, 2000.



This page intentionally contains only this sentence.

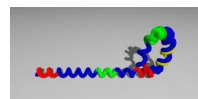
Summaries

Summary

Single-Molecule Techniques in Biological and Biophysical Research

The rapid developments in the field of optical imaging and detection have led to a wealth of new methods which allow us to study matter on the molecular and even atomic level. While this makes it possible to visualize the structure of proteins and the organization of biological structures *in vitro*, and has provided answers to many issues, it has also raised new questions about the interaction of proteins with each other and their dynamics *in vivo*.

In my thesis I introduce several applications of single molecule techniques, mostly based on fluorescence microscopy. Chapter 2 concerns characterization of autofluorescent proteins in bulk for the case of two-photon excitation. Two-photon excitation is a non-linear process in which the energy needed to excite a fluorophore is taken from the absorption of two photons, each carrying half the needed energy, within a very short time ($\approx 10^{-15}$ s). Despite the fact that this process is very rare, expressed in cross-sections, $\sigma^{(2)} \sim 10^{-50}$ cm⁴s/photon versus the one-photon case



SUMMARIES

$\sigma^{(1)} \sim 10^{-16} \text{ cm}^2$, it can be observed using a pulsed laser, generating ultra-short (100 fs) bursts of near-infrared light. The possible advantages of this method are the low absorption in tissue, allowing us to penetrate several millimeters into a specimen, and the low background expected due to the use of near-IR excitation wavelengths. Autofluorescent proteins proved to be excellent fluorophores in terms of two-photon absorption, yet their rapid photobleaching does not allow their use as single-fluorophore markers under these conditions.

Chapter 3 reports on true single molecule measurements using autofluorescent proteins as markers to study the aggregation of the β_2 adrenergic receptor ($\beta_2\text{AR}$). The $\beta_2\text{AR}$, a member of the large family of G-Protein-Coupled Receptors (GPCR), was one of the first GPCR to be sequenced and serves as widely accepted model system. It plays an important role in the regulation of blood-pressure and the dilation of the bronchia, and it can also be found in muscle tissue, the kidneys, the liver, and the pancreas. In biochemical assays GPCRs are regularly detected as dimers, and a connection between the formation of dimers and the functionality of the receptors has been suggested. Our aim in this study was, therefore, to assess the degree of dimerization of the $\beta_2\text{AR}$ -eYFP-fusion-protein in a mammalian cell prior to stimulation, and compare this data to the stoichiometry of the receptor after stimulation with the agonist (-)isoproterenol and its biologically inactive stereoisomer. To reach this goal we had to use the previous characterization of eYFP intensity and bleaching behavior to model the time dependent shift in intensity of oligomeric receptors in membranes, and apply the result to the data found in our experiments. Indeed, our results show that the initially dimeric $\beta_2\text{AR}$ forms larger aggregates within

one minute after stimulation. These aggregates stay stable for at least 10 minutes. The negative control with the biologically inactive stereoisomer caused a shift toward monomeric intensities, which can be explained by photobleaching.

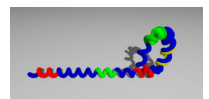
Chapter 4 describes the adaptation of our highly sensitive single-molecule setup to allow the separation-free detection of Rolling Circle Replication (RCR) Products against the background of free, fluorescent labels.

RCR is a new and very specific way to test for the presence of DNA sequences. If a matching DNA-sequence is found by a so-called padlock-probe, this probe can form a circle. DNA-polymerase can copy this probe and, due to the circular form, will produce a long piece of DNA consisting of repeats of the padlock motif (“rolling”). Special labels recognizing this padlock motif can bind to the RCR product, causing a locally increased signal, which allows us to detect the RCR product without the need to first remove all unbound probes.

Finally, in chapter 5 a previous method allowing dual-color detection is extended to allow for simultaneous recording of images and emission spectra of small fluorescent particles. For this, a blazed reflection grating is introduced into the beam path. Unlike its conventional counterpart, a blazed grating allows one to choose and influence the distribution of energy between the different diffraction orders.

We applied this new technique to test samples of 20 nm fluorescent beads, membrane fragments containing photosynthetic complexes, and for the unequivocal identification of chromosomes using a COBRA-FISH¹ label.

¹COmbined Binary RAtio Fluorescence In-Situ Hybridization



Samenvatting

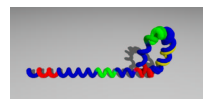
Technieken voor de observatie van individuele moleculen en hun toepassing in biologisch en biofysisch onderzoek

De voortdurende ontwikkelingen op het gebied van optische detectie hebben geresulteerd in een groot aantal nieuwe technieken, die wetenschappers toegang geven tot het niveau van enkele atomen of moleculen. Hierdoor is het mogelijk geworden de structuur van eiwitten en de organisatie van biologische systemen *in vitro* te visualiseren. Deze nieuw verworven kennis heeft veel vragen beantwoord, maar heeft ook nieuwe vragen over de dynamica en de interacties van eiwitten *in vivo* opgeroepen.

In mijn proefschrift introduceer ik toepassingen van technieken voor het visualiseren van individuele moleculen, die voornamelijk gebaseerd zijn op fluorescentie microscopie. Hoofdstuk 2 beschrijft de fotofysische karakterisering van autofluorescente eiwitten in bulk bij twee-fotonen excitatie. Twee-fotonen excitatie is een niet-lineair proces waarin de energie die nodig is om een fluorofoor aan te slaan afkomstig is van de absorptie van twee fotonen, waarbij beide fotonen de helft van de benodigde energie bijdragen. Dit proces vindt plaats op een tijdschaal van 10^{-15} s. De waarschijnlijkheid van dit proces komt tot de uitdrukking in de absorptie doorsnede, die in het geval van twee-fotonen absorptie $\sigma^{(2)} \sim 10^{-50}$ cm⁴s bedraagt, terwijl het in het een-fotonen geval $\sigma^{(1)} \sim 10^{-16}$ cm² bedraagt. Het fenomeen van twee-fotonen excitatie kan geobserveerd worden door gebruik te maken van een laser die ultrakorte 100 femtoseconden pulsen uitzendt met een golflengte die in het nabij-infrarood ligt. De veronderstelde voordelen van deze methode zijn een lage absorptie in organisch weefsel waardoor het moge-

lijk wordt enkele millimeters in het weefsel door te dringen. Daarnaast is de verwachte achtergrond laag door het gebruik van excitatie golflengtes in het nabije infrarood. Autofluorescente eiwitten bleken fluoroforen van hoge kwaliteit te zijn waar het gaat om twee-fotonen absorptie, maar de snelle fotobleiking die optreedt maakt het onmogelijk ze te gebruiken voor studies op het niveau van enkele fluoroforen.

Hoofdstuk 3 behandelt een experiment toegepast op enkele moleculen. In dit experiment hebben wij autofluorescente eiwitten gebruikt als markers om de aggregatie van β_2 adrenerge receptoren (β_2 AR) te bestuderen. Deze receptor is onderdeel van de grote familie van G-eiwit-gekoppelde receptoren (GPCRs). De β_2 adrenerge receptor was een van de eerste GPCRs waarvan de sequentie bekend was en dient als een algemeen geaccepteerd modelsysteem. De β_2 AR speelt een belangrijke rol in de regulering van de bloeddruk en verwijding van de bronchia. De receptor komt voor in verschillende weefsels zoals spierweefsel en organen zoals nier, lever en alveesklier. In biochemische proeven worden G-eiwit-gekoppelde receptoren over het algemeen in de vorm van dimeren gevonden. Een verband tussen de vorming van dimeren en de functionaliteit van de receptor wordt al langere tijd gesuggereerd. Het doel van mijn onderzoek was dan ook de mate van dimerisatie van het β_2 AR-eYFP fusie-eiwit in zoogdiercellen te bepalen, waarbij ook de invloed van stimulatie van de receptor door zijn ligand bekeken is. Om dit te bestuderen hebben wij gebruik gemaakt van de eerdere karakterisatie van de intensiteitsverdeling en het bleekgedrag van eYFP om de tijdsafhankelijke verschuiving van de intensiteit van geoligomereerde receptoren in membranen te modelleren. Het resultaat van deze modellering hebben wij gebruikt voor de analyse van de data die voort-



kwam uit onze experimenten. Onze resultaten laten zien dat de, in eerste instantie als dimeer voorkomende, β_2AR grote aggregaten vormt binnen een minuut na stimulatie. Deze aggregaten blijven tenminste 10 minuten stabiel. Proeven met een biologisch inactieve stereo-isomeer van het ligand als negatieve controle laten een verschuiving naar intensiteiten karakteristiek voor een monomeer zien. Deze verschuiving kan verklaard worden door het verschijnsel fotobleken.

Hoofdstuk 4 beschrijft de aanpassingen die wij aan onze opstelling hebben moeten aanbrengen, om de detectie van “Rolling Circle Replication” (RCR) producten mogelijk te maken tegen een achtergrond van fluorescente labels in oplossing, zonder zuivering van het monster te vereisen. RCR is een nieuwe en specifieke manier om de aanwezigheid van unieke DNA-sequenties te testen. Als combinatie met een passende DNA-sequentie is opgetreden wordt het mogelijk voor de “padlock”-probe om enkelstrands, circulair DNA te vormen. Dit maakt het mogelijk voor DNA-polymerase om kopiën van deze probe te maken. De cirkelvorm bevordert de productie van lange stukken DNA (“rolling”), waarin de gezochte sequentie meerdere malen voorkomt. Speciale labels die deze sequentie herkennen kunnen aan het RCR product binden, waardoor lokaal een hoog signaal ontstaat, tegen de achtergrond van de ongebonden labels.

Ten slotte wordt in hoofdstuk 5 beschreven hoe de methode waarmee twee kleuren detectie kan worden toegepast, wordt uitgebreid om gelijktijdig zowel een plaatje als een emissie-spectrum van een klein fluorescent object te verkrijgen. Hiervoor wordt een *blazed* reflectie-tralie in het emissiepad geplaatst. Anders dan bij conventionele tralies is het met deze tralie mogelijk om de verdeling van energie tussen de verschillende diffractie-orde

te kiezen en beïnvloeden. Wij hebben deze nieuwe techniek toegepast op fluorescente bolletjes met een doorsnede van 20 nm, en membraan fragmenten die fotosynthetische complexen bevatten. Daarnaast kunnen wij met deze methode de verschillende COBRA-FISH² gelabelde chromosomen on-dubbelzinnig identificeren.

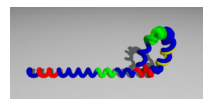
Zusammenfassung

Einzelmolekül-Techniken in der biologischen und biophysikalischen Forschung

Die rasante Entwicklung auf dem Gebiet der optischen Mikroskopie resultierte in einer Vielzahl neuer Techniken, die die Betrachtung von Objekten auf der Größenskala von einzelnen Atomen und Molekülen erlauben. Dadurch ist es möglich geworden, die Struktur von Proteinen und die Organisation biologischer Systeme *in vitro* zu visualisieren. Die Kenntnis der biologischen Struktur half viele Fragen zu beantworten, hat aber zugleich weiterreichende Fragestellungen über z.B. die Dynamik von Proteinen *in vivo* und die Wechselwirkung zwischen Proteinen aufgeworfen.

In meiner Dissertation stelle ich einige Anwendungen dieser neuen Techniken zur Untersuchung von Einzelmolekülen vor. Die Techniken basieren hauptsächlich auf der Fluoreszenz-Mikroskopie. In Kapitel 2 beschreibe ich Experimente zur Charakterisierung von autofluoreszenten Proteine in Lösung unter Zwei-Photonen-Anregung. Die Zwei-Photonen-Anregung ist ein nicht-linearer Prozess, bei dem ein Fluorophor die Anregungsenergie E durch die Absorption von zwei Photonen mit der jeweils halben Ener-

²COmbined Binary RAtio Fluorescence In-Situ Hybridization



gie $E/2$ erhält. Dies geschieht auf einer Zeitskala von etwa 10^{-15} s. Die Wahrscheinlichkeit für diesen Prozess wird durch den “Absorptionsquerschnitt” σ beschrieben. Der Absorptionsquerschnitt für die Zwei-Photonen-Absorption beträgt $\sigma^{(2)} \sim 10^{-50} \text{ cm}^4\text{s}$, wogegen der Wert für “gewöhnliche” Ein-Photonen-Absorption bei $\sigma^{(1)} \sim 10^{-16} \text{ cm}^2$ liegt. Durch den Gebrauch eines Lasers, welcher ultra-kurze (100 fs)³, intensive Pulse im nahen infraroten Spektralbereich produziert, ist es möglich, einen solchen Zwei-Photonen-Übergang zu induzieren. Die potentiellen Vorteile der Methode liegen in der geringen Absorption von infrarotem Licht, wodurch es möglich ist, einige Millimeter tief in intaktes Gewebe einzudringen. Des Weiteren ist bei dieser Anregungswellenlänge auch ein äußerst geringes Hintergrundsignal zu erwarten. Meine Studien zeigen, dass die autofluoreszenten Proteine ausgezeichnete Farbstoffe sind. Allerdings macht es ihre kurze Bleichzeit beinahe unmöglich, sie für Einzel-Molekül Studien zu gebrauchen.

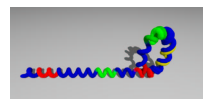
In Kapitel 3 beschreibe ich ein Experiment, in dem autofluoreszente Proteine zur Untersuchung der Aggregation von β_2 adrenergen Rezeptoren ($\beta_2\text{AR}$) eingesetzt wurden. Diese Rezeptoren sind Teil der en Familie der G-Protein-Gekoppelten Rezeptoren. Der $\beta_2\text{AR}$ war einer der ersten dieser Familie, dessen Sequenz analysiert werden konnte. Daher dient er als ein allgemein akzeptiertes Modellsystem. Der $\beta_2\text{AR}$ spielt eine wichtige Rolle in der Regulierung des Blutdrucks und der Erweiterung der Bronchien. Der Rezeptor kommt in vielen verschiedenen Geweben und Organen, wie der Niere, Leber und Bauchspeicheldrüse vor. In biochemischen Versuchen werden G-Protein-Gekoppelte Rezeptoren im Allgemeinen in Form von Dimeren gefunden. Geraume Zeit wird ein Zusammenhang zwischen der Dimerisie-

³Eine Femtosekunde entspricht 0.000'000'000'000'001 Sekunden.

rung und der Funktion vermutet. Es war Teil meiner Forschung, die Dimerisierung eines β_2 AR-eYFP Fusions-proteins in abhängigkeit der Stimulierung des Rezeptors zu messen. Dafür habe ich zunächst die Fluoreszenz-Intensitätsverteilung und das Bleichverhalten von eYFP charakterisiert. Die zeitabhängige Verschiebung der Intensitätsverteilung von Rezeptor-oligomeren wurde danach modelliert. Wie erwartet, zeigen meine Resultate, dass der hauptsächlich als Dimer vorkommende β_2 AR schon wenige Minuten nach der Aktivierung große Aggregate formt. Diese Aggregate bleiben bis zu 10 Minuten lang stabil. Kontrollexperimente mit einem biologisch inaktiven Stereo-Isomer des Liganden des Rezeptors zeigen eine Verschiebung der Intensitätsverteilung hin zu Monomeren, was sich als Effekt des Photobleichens erklären lässt.

Kapitel 4 behandelt die Modifikation unseres Einzel-Molekül Aufbaus für die Detektion von “Rolling Circle Replication” (RCR) DNS Produkten. Mit dem veränderten Aufbau ist es möglich, die DNS-Produkte auch in einem hohen Hintergrund von freien fluoreszenten Labeln in Lösung zu detektieren, ohne dass ein Reinigungsschritt erforderlich ist. RCR ist ein neuartiger DNS-Test, der mit großer Verlässlichkeit die Anwesenheit spezifischer DNS-Sequenzen nachweisen kann. Wenn ein besonderes DNS-“Padlock” (“Vorhangschloss”) an seine komplementäre Sequenz bindet, wandelt er sich mit Hilfe einer Ligase zu einer kreisförmigen DNS-Struktur um. Diese kann wiederum durch eine DNS-Polymerase “abgerollt” werden, d.h. es entsteht ein langer Strang von DNS, der aus Kopien der “Padlock”-Sequenz besteht. Mehrere DNS-Label können nun gleichzeitig an dieses RCR-Produkt binden, was die Detektion des DNS-Stranges möglich macht.

Im letzten Kapitel 5 wird eine Methode beschrieben, mit der gleich-



zeitig das Bild und ein Emissionsspektrum von fluoreszierenden Objekten aufgenommen werden kann. Dafür wird ein *blazed* Gitter in den Strahlengang des Mikroskops eingeführt. Anders als bei gewöhnlichen Gittern ist es dabei möglich, die Signalstärke in den Beugungsordnungen zu beeinflussen. Wir haben diese neue Methode zunächst an verschieden 20 nm grossen Latexkügelchen getestet, die mit zwei unterschiedlichen Fluoreszenz-Labeln markiert waren. Des Weiteren habe ich diese Methode weiter ausgebaut um Chromosomen mittels sogenannter COBRA-FISH⁴ Label eindeutig zu identifizieren.

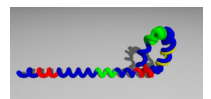
⁴COmbined Binary RAtio Fluorescence In-Situ Hybridization

Curriculum Vitae

I was born on November 7, 1973, in the town of Wels, Austria. I grew up in Linz, where I earned my “Matura” at the Bundesrealgymnasium Landwiedstraße in 1992.

After eight months service in the Austrian armed forces, I begun my study of Technical Physics at the Johannes Keppeler Universität in Linz in autumn 1993. I was elected student representative in the faculty council for two two-year terms and I also got involved in politics both on the campus as well as the city council as member of the now defunct Liberal Party, where I had to realize that some people conduct political debate in a only marginally less violent way than a full-contact sport. I graduated from the University of Linz with a degree in Physics and the specialization “Biophysics” in November 1999.

During my four year as PhD student in the group of Prof. Thomas Schmidt in Leiden I have had the opportunity to present the results of my research – in the form of a poster – at the ‘Frühjahrstagung der Deutschen Physikalischen Gesellschaft, Potsdam, March 2000, the 3rd European Biophysical Congress, München, September 2000, the International Workshop “Single Molecule Detection and Ultra-Sensitive Analysis in Life Science”

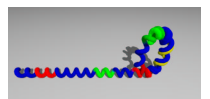


CURRICULUM VITAE

(Picoquant), Berlin, and the Biophysical Society Annual Meeting. I have been invited to the Symposium of the Daresbury Laboratory, Daresbury, UK, to give a talk “Single Molecule Methods in Biophysical Research”, and I am gratefully acknowledging support by the NWO-SMRC Travel-grant 910-31-402, which allowed me to visit the group of Dr. Mats Nilsson at the Rudbeck Laboratories, Uppsala, Sweden.

Nawoord

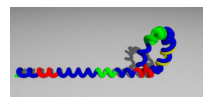
Dit nawoord is met opzet wit gelaten.



This page intentionally contains only this sentence.

List of Tables

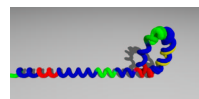
1.1	Resolution of optical microscopes	2
1.2	Rate Constants for several fluorophores	7
2.1	TPE action cross-sections	41
2.2	Detection Ratio of the Autofluorescent Proteins	42
3.1	Fitting oligomeric populations	63



This page intentionally contains only this sentence.

List of Figures

1.1	Jabloński diagram of a fluorophore	6
1.2	Molecular Model of GFP	14
1.3	Molecular Model of a GPCR	17
1.4	Schematics of COBRA-FISH	20
1.5	Labeling with artificial fluorophores	22
1.6	Hydromedusa <i>Aequorea victoria</i>	23
1.7	Coral <i>Discosoma</i> sp	24
1.8	Schematic of a RCR reaction	25
2.1	Square Dependence of Fluorescence on the Laserpower . . .	43
2.2	σ_{TPE} of the Autofluorescent Proteins	44
2.3	σ_{TPE} of cellular autofluorescence	45
2.4	Two-Photon induced bleaching of eGFP in cells	46
3.1	Transfected cells and single β_2 AR on HEK293 cells	64
3.2	β_2 AR aggregates upon stimulation	65
3.3	Demonstration of fit	66
3.4	Simulation results for oligomeric β_2 AR	67



LIST OF TABLES

3.5	Multistep bleaching of β_2 AR aggregates	68
4.1	Schematic representation of the setup	83
4.2	RCR product traces	84
4.3	Intensity Distribution of the labelled DNA	85
4.4	Subtraction of Static Background	86
4.5	Comparision of Data before and after Background Subtraction	87
4.6	RCR Two Colour Experiments	88
5.1	Experimental Setup	101
5.2	Spectra of fluorescent beads	102
5.3	Spectra of COBRA-FISH-stained Mouse Chromosomes . . .	103